

AI reconstruction of European weather from the Euro-Atlantic regimes

Alessandro Camilletti¹ | Gabriele Franch¹ | Elena Tomasi¹ | Marco Cristoforetti¹

¹Data Science for Industry and Physics, Fondazione Bruno Kessler, via Sommarive 18, 38123, Trento (TN), Italy

Correspondence

Alessandro Camilletti, Data Science for Industry and Physics, Fondazione Bruno Kessler, via Sommarive 18, 38123, Trento (TN), Italy
Email: acamilletti@fbk.eu

Funding information

ICSC-Centro Nazionale di Ricerca in High Performance Computing, Big Data and Quantum Computing, Spoke4 - Earth and Climate, funded by European Union - NextGenerationEU.

We present a non-linear AI model designed to reconstruct monthly mean anomalies of the European temperature and precipitation based on the Euro-Atlantic WR indices. WR represent recurrent, quasi-stationary, and persistent states of the atmospheric circulation that exert considerable influence over the European weather, therefore offering an opportunity for sub-seasonal to seasonal forecasting. While much research has focused on studying the correlation and impacts of the WR on European weather, the estimation of ground-level meteorological variables, such as temperature and precipitation, from Euro-Atlantic WR remains largely unexplored and is currently limited to linear methods. The presented AI model can capture and introduce complex non-linearities in the relation between the WR indices, describing the state of the Euro-Atlantic atmospheric circulation and the corresponding surface temperature and precipitation anomalies in Europe. We discuss the AI-model performance in reconstructing the monthly mean two-meter temperature and total precipitation anomalies in the European winter and summer, also varying the number of WR used to describe the monthly atmospheric circulation. We assess the impact of errors on the WR indices in the reconstruction and show that a mean absolute relative error below 80% yields improved seasonal reconstruction compared to the ECMWF operational seasonal forecast system, SEAS5. As a demonstration of practical applicability, we evaluate the model using WR indices predicted by SEAS5, finding slightly better or comparable skill relative to the SEAS5 forecast itself. Our findings demonstrate that WR-based anomaly reconstruction, powered by AI tools, offers a promising pathway for sub-seasonal and seasonal forecasting.

Keywords Euro-Atlantic regimes, seasonal prediction, artificial intelligence, circulation patterns, reconstruction

1 | INTRODUCTION

Predicting atmospheric conditions for the upcoming season is crucial in various social and economic applications. Accurate seasonal forecasts can guide agricultural planning, allowing farmers to optimize crop selection, planting, and harvesting schedules, supporting food security and market stability (Ceglar and Toreti, 2021). In the energy sector, such forecasts help anticipate demand fluctuations, aiding in efficient resource allocation and grid management (Dorrington et al., 2020; Buonocore et al., 2022; El-Azab et al., 2025). Additionally, governments and disaster preparedness agencies can use reliable forecasts to mitigate the impacts of extreme weather events, such as droughts or floods, thereby reducing economic losses and protecting vulnerable communities (Alferi et al., 2013; Samaniego et al., 2019). Despite recent advances, forecasting European weather on long-term timescales remains challenging for both dynamical (Palmer et al., 2004; Mishra et al., 2019) and statistical methods (Krikken et al., 2024). While the weather forecast of physics-based numerical weather prediction (NWP) is limited to about two weeks due to the intrinsic chaotic nature of the atmosphere (Lorenz, 1963), statistical methods can explicitly leverage slowly varying, persistent, and more predictable components of the Earth system. By Rossby wave propagation, these large-scale phenomena give rise to teleconnection patterns between distant regions of the Earth (Wallace and Gutzler, 1981; Ambrizzi et al., 1995), opening a window of opportunity to enlarge the forecast horizons. In the northern hemisphere, the main mode of atmospheric variability, represented by the North Atlantic Oscillation (NAO) (Hurrell et al., 2003), or the strongly related Arctic Oscillation (AO), exerts influence over North America, Europe and part of Asia (Deser et al., 2017; Trigo et al., 2002), and is characterized by a typical persistence of 10 to 30 days (Feldstein, 2003; Rennert and Wallace, 2009; Roberts et al., 2023).

The existence of persistent modes of the atmospheric state suggests that large-scale atmospheric circulation can be systematically decomposed into a finite number of dominant states (Rossby, 1940).

Weather regimes (WR), first introduced by Rex (1951), are recurrent, quasi-stationary, and persistent states of atmospheric circulation (Hochman et al., 2021). WR may be defined separately for the summer and winter seasons, in which case four WR are optimal in the Euro-Atlantic sector (Michelangeli et al., 1995), or over the entire year, in which case seven WR are optimal (Grams et al., 2017). In the Euro-Atlantic sector, the WR are strongly related to the NAO (Michelangeli et al., 1995) and are known to exert considerable influence over the European weather (van der Wiel et al., 2019; Trigo and DaCamara, 2000; Plaut and Simonnet, 2001; Hall and Hanna, 2018; Simpson et al., 2024)¹. Their persistent nature (see e.g. Strommen et al., 2023; Mukhin et al., 2024b, for a related discussion), often influenced by teleconnection patterns (Roberts et al., 2023; Michel and Rivière, 2011), opens up the possibility of extending the forecast horizon in Europe beyond the limit posed by the chaotic nature of the atmosphere (Ferranti et al., 2015, 2018). This justifies the increasing interest in assessing the capability of NWP (Ferranti et al., 2018; Büeler et al., 2021) and Artificial Intelligence (AI) models based on Neural Networks (NN) architectures to forecast the transitions between large-scale circulation regimes in the sub-seasonal and seasonal timescales. In the sub-seasonal scale, deep learning models such as convolutional neural networks (CNNs) and recurrent neural networks (RNNs) have been successfully applied to enhance large-scale circulation regimes by capturing complex spatial and temporal dependencies in reanalysis data (Chattopadhyay et al., 2020; Nielsen et al., 2022). Bommer et al. (2025) introduce advanced machine learning approaches to improve sub-seasonal predictions of the WR by leveraging teleconnection patterns, further enhancing forecast reliability and skill. On the seasonal scale, Hall et al. (2019) use complex modeling techniques to address the data-scarce conditions typical of this scale, aiming to forecast the first three principal components derived from empirical orthogonal function (EOF) analysis in the North Atlantic region.

However, while much research has focused on the

¹Some of the works mentioned here refer to different large-scale circulation patterns than WR, but share similar ideas and comparable results.

evaluation of the forecast and on the impacts of the WR on the European weather, the estimation of ground-level climate variables, such as temperature and precipitation, from Euro-Atlantic WR remains largely unexplored and limited to linear methods, e.g. considering the mean surface weather variables associated with the dominant regime (Madonna et al., 2021; Roberts et al., 2023). Additionally, Gerighausen et al. (2024) highlight the importance of intra-regime variability and suggest the use of continuous WR indices to capture the regimes ‘subflavours’ in place of the categorical classification commonly found in the literature (Madonna et al., 2021; Grams et al., 2017; Plaut and Simonnet, 2001; Trigo and DaCamara, 2000).

In this study, we present two AI models designed to reconstruct monthly anomalies in European temperature or precipitation, based on knowledge of the WR indices. The models can capture and introduce complex non-linearities in the relationship between the WR indices, which describe the state of the Euro-Atlantic atmospheric circulation, and the corresponding two-meter temperature and precipitation anomalies in Europe. After presenting the datasets (Sec. 2) and defining the WR and the target fields (Sec. 3), we present the AI model’s architecture in Sec. 4. We evaluate its accuracy in reconstructing monthly mean temperature and total precipitation anomalies in winter and summer (Sec. 5.1) and compare it with a standard baseline, namely the linear regression on individual WR (Sec. 5.2). We then discuss the impact of changing the number of indices used to represent the atmospheric circulation (Sec. 5.3). Given the potential future applications in a real forecasting scenario, we discuss the effects of introducing errors in the WR indices, establishing a lower bound on the WR prediction accuracy required to outperform the European Center for Medium-Range Weather Forecasts (ECMWF) operational seasonal forecast system, SEAS5 (Sec. 5.4). In other words, we utilize the presented AI models as a mapping from the WR indices to the anomalies of interest to address the following questions:

- How does the model’s reconstruction performance degrade as the number of input indices is reduced?

- To what level of accuracy must the seven WR indices be forecasted to outperform SEAS5 in predicting seasonal mean two-meter temperature and total precipitation?

We also test the accuracy of the AI models in reconstructing the targeted anomalies using the SEAS5 forecast of the winters and summers WR indices (Sec. 5.5) as a first evaluation of the models in a concrete forecasting scenario.

In summary, the AI models presented here offer a promising approach to AI-driven long-range weather forecasting by leveraging the predictability of large-scale atmospheric circulation and its relation with surface-level variables. The models demonstrate good reconstruction capability, as well as notable adaptability and stability in the presence of errors in the WR indices, underlining their potential for seasonal forecasting applications. While they are applied in this study to reconstruct two-meter temperature and total precipitation anomalies on a monthly timescale, the architecture is sufficiently flexible to be adapted to other regions and variables without modification. Additionally, the model’s relatively lightweight design enables efficient training (requiring a single GPU), further supporting its practicality for broader implementation.

2 | DATASETS

2.1 | ERA5 reanalysis

ERA5, the fifth generation of ECMWF global reanalysis (Hersbach et al., 2020), is the current state-of-the-art reanalysis and the most widely used data set in climate sciences. The ERA5 reanalysis spans years from 1940 onward, with a latency of 5 days and a Cartesian grid resolution of 0.25° , corresponding to approximately 31 km horizontal resolution at the equator. Using a bilinear interpolation, we upscaled the ERA5 data from the original $0.25^\circ \times 0.25^\circ$ Cartesian grid to a $1^\circ \times 1^\circ$ Cartesian grid.

The geopotential height (GPH) is one of the most widely used variables for studying teleconnections and decomposing atmospheric circulation into a set of

dominant modes. We use the daily mean GPH at 500 hPa (Z500) in the Euro-Atlantic region (80°W to 40°E, 30°N to 90°N) to compute the WR and the related WR indices (see Sec. 3.1) used as input in our models. The work aims to reconstruct the monthly mean two-meter temperature and total precipitation anomalies in Europe (i.e., within the domain 20°W to 30°E, 35°N to 70°N). We use the daily mean two-meter temperature and daily total precipitation to compute the respective daily anomalies, which are then aggregated monthly (see Sec. 3.3).

2.2 | Numerical seasonal forecast: SEAS5

SEAS5 is the fifth-generation seasonal forecasting system developed by ECMWF (Johnson et al., 2019). It provides global, long-range forecasts up to seven months ahead, using an advanced coupled ocean-atmosphere model. The SEAS5 forecast and hindcast of monthly aggregated GPH at 500 hPa, two-meter temperature, and precipitation with 25 ensemble members were retrieved from the Copernicus Data Store (CDS) in the months from January 1981 to December 2024 on a 1°×1° regular grid over the Euro-Atlantic region previously defined.

3 | PRE-PROCESSING

The following section details the pre-processing steps employed to derive the input and target variables for the AI models. We then describe the models' architecture, training and evaluation in Sec. 4.

3.1 | Input of the AI-model: weather regimes indices

There are different methods of extracting low-frequency modes of variability of the atmospheric circulation (refer to Hannachi et al., 2017; Schlef et al., 2019; Mukhin et al., 2024a; Spuler et al., 2024, for some examples). In this work, we use the method presented in Grams et al. (2017), a natural extension of the procedure discussed in Ferranti et al. (2015). The following briefly recaps

the procedure for obtaining the seven year-round WR (Grams et al., 2017; Büeler et al., 2021).

The daily Z500 field is post-processed at each latitude ϕ and longitude λ of the Euro-Atlantic sector to obtain the standardized anomaly field, $\Phi(t, \lambda, \phi)$:

1. The climatology period is defined as the days from the first of January of 1981 to the end of 2010
2. The calendar day climatology is obtained by applying a 15-day moving window centered on each calendar day (± 7 days) in the climatology period;
3. The calendar day climatology is subtracted from the Z500 field, obtaining the Z500 anomalies, $\Phi(t, \lambda, \phi)$;
4. The resulting field is 5 days low-pass filtered using a Savitzky-Golay filter²;
5. A calendar day normalization is computed by applying to the Z500 calendar standard deviation a 15-day moving window centered on each calendar day (± 7 days) in the climatology period, and then taking the spatial average on the full domain;
6. The Z500 anomaly field, $\Phi(t, \lambda, \phi)$, is divided by the calendar day normalization.

The last step is necessary to remove the seasonal cycle in the Z500 anomaly field amplitude, and it is required to define the year-round WR (Grams et al., 2020). EOF analysis (Hannachi et al., 2007; Rieger and Levang, 2024) is performed on the standardized daily anomalies in the climatology period over the Euro-Atlantic domain. We retain the first seven EOF, explaining $\approx 74\%$ of the total variance. K-means clustering is performed on the top seven principal components (PCs), yielding seven cluster centroids. The climatology mean of the Z500 field and Z500 anomalies³ associated with each cluster are shown in Fig. 1. The seven clusters mean correspond to the seven year-round Euro-Atlantic WR, with three cyclonic regimes: Atlantic Trough (AT), Zonal Regime (ZO), and Scandinavian Trough (ST); and four blocking regimes: Atlantic Ridge (AR), Euro-

²In agreement with Robertson et al. (2020) and Lee et al. (2023), we did not find significant differences between the low-pass filtered and non-filtered WR.

³although the clustering and the rest of the analysis are performed on the normalized anomalies, in the figure the non-normalized anomalies (i.e., the anomalies obtained in step 3) are shown for comparison with previous works.

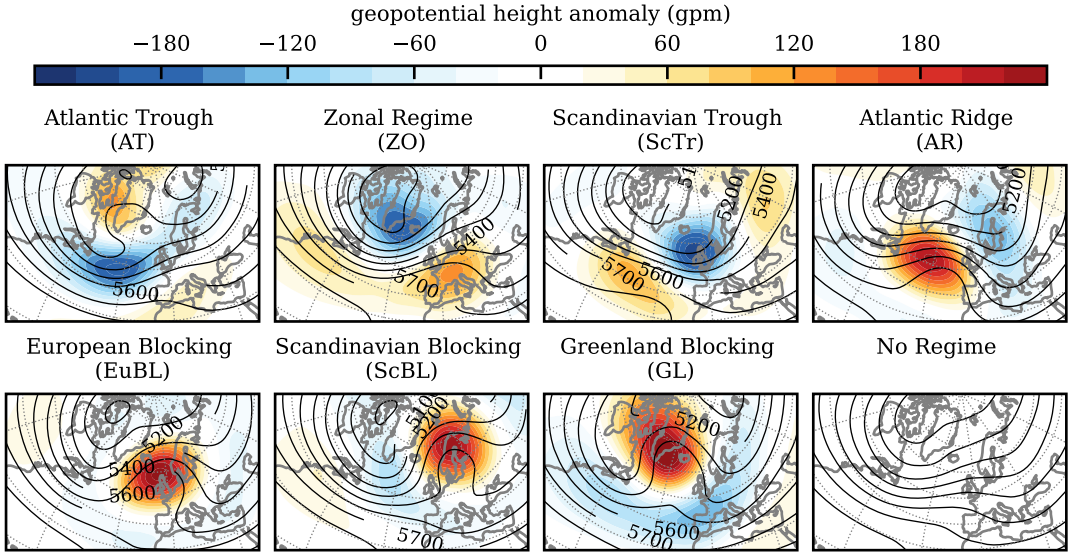


FIGURE 1 Cluster mean of the Z500 field (black isocontours) and corresponding average Z500 anomalies in winter (December, January, February), associated with the seven year-round Euro-Atlantic WR. The average is performed in the 1981-2010 climatology. The “No Regime” refers to the mean atmospheric circulation when there is no WR attribution according to the index life-cycle criteria (Grams et al., 2017).

pean Blocking (EuBL), Scandinavian Blocking (ScBL) and Greenland Blocking (GL). The “No Regime” refers to the mean atmospheric circulation when there is no WR attribution: the attribution of each day to one of the WR is subject to life-cycle criteria (see (Grams et al., 2017) for the details).

The WR index, I_{wr} , is defined as the normalized projection of the daily standardized anomaly field, $\tilde{\Phi}(t, \lambda, \phi)$, onto each cluster mean field, $\tilde{\Phi}_{wr}(\lambda, \phi)$, where $wr = (\text{AT}, \text{ZO}, \text{ST}, \text{AR}, \text{EuBL}, \text{ScBL}, \text{GL})$:

$$I_{wr}(t) = \frac{P_{wr}(t) - \langle P_{wr}(t) \rangle}{\sqrt{\langle (P_{wr}(t) - \langle P_{wr}(t) \rangle)^2 \rangle}}, \quad (1)$$

where the averages $\langle \cdot \rangle$ are performed in the climatology period, and P_{wr} is the aforementioned projection (see Michelangeli et al., 1995):

$$P_{wr}(t) = \frac{1}{\sum_{\lambda, \phi} \cos \phi} \sum_{\lambda, \phi} \tilde{\Phi}(t, \lambda, \phi) \tilde{\Phi}_{wr}(\lambda, \phi) \cos \phi \quad (2)$$

The method outlined here for deriving the seven WR

differs slightly from that used in Grams et al. (2017) and Büeler et al. (2021). Key differences are detailed in Appendix B.

We are interested in quantifying the performance of the AI models in reconstructing the targeted anomalies by changing the number of WR used as input. Therefore, in addition to the seven weather regimes, we use the same procedure described before for the winter (December, January, February - DJF) and summer (June, July, August - JJA) seasons separately, changing the number of clusters to four. The four weather regimes obtained are the AT, the ScBL, the ZO, and the GL in winter (Fig. A.1), and in summer (Fig. A.2). We also compute the NAO index (Hurrell et al., 2003) separately for the summer and winter seasons, as the principal component (PC) of the first EOF. The analysis is performed on the same Euro-Atlantic region and the same climatology period used to compute the WR.

Finally, we aggregate the I_{wr} on a monthly basis. Indeed, we use the monthly average of the seven or four I_{wr} as an input variable in our AI models (see Sec. 4).

3.2 | Perturbed indices

As previously mentioned, it is valuable to assess the model's performance when using perturbed indices that simulate forecasting errors. This reflects a realistic scenario in which the predicted indices are not perfectly accurate.

Let us indicate with I'_{wr} the set of indices with errors. The mean absolute error (MAE) between I_{wr} and I'_{wr} is a dimensionless number that depends on the normalization of the anomalies and the normalization of the WR index itself. We then define the mean absolute relative error (MARE) as $\langle |I_{wr} - I'_{wr}| / |I_{wr}| \rangle$, which quantifies the typical absolute relative error between the correct index I_{wr} and the perturbed index I'_{wr} . We want to produce a perturbed index I'_{wr} for a given value of the MARE. For this purpose, let us define $I'_{wr} = (1 + f_{wr})I_{wr}$, where $f_{wr} \sim N(0, \sigma)$ are random variables sampled from a normal distribution with mean zero and standard deviation σ . It follows that the mean error is zero by construction. In other words, there is no bias in the I'_{wr} error. The MARE is $\langle |f_{wr}| \rangle = \sqrt{2/\pi} \sigma$. Fixing the distribution of f_{wr} , that is, the value of σ , for a given value of the MARE is straightforward. Also note that, since f_{wr} and I_{wr} are independent, the MAE of the perturbed indices, $\langle |I_{wr} - I'_{wr}| \rangle$, is simply given by $\text{MARE} \times \langle |I_{wr}| \rangle$. Unlike MARE, the MAE, therefore, depends directly on the statistical properties of the original indices.

For every value of the MARE from 0 to 160%, we compute 50 random realization of I'_{wr} sampling from $I_{wr} \times N(0, \sqrt{\pi/2} \text{MARE})$. Each realization is then passed as an input to the AI models (see Sec. 4) to obtain an estimate of the monthly average two-meter temperature and total precipitation in Europe for the months from January 2011 to December 2024.

3.3 | Target fields: temperature and precipitation anomalies

The daily two-meter temperature and total precipitation anomalies are computed following the same procedure at points 1 to 3 described in Sec. 3.1. Following the same pre-processing, the relevant relations between WR and

target anomalies are preserved, allowing the AI models to exploit them for the reconstruction. Note that we do not normalize the anomalies by the calendar standard deviation, so we express the anomalies in Kelvin (K) for the monthly mean two-meter temperature and in centimeters (cm) for the monthly total precipitation.

The daily variables are then aggregated monthly: the daily mean two-meter temperature anomaly is averaged over every day in the month, while the daily total precipitation anomaly is summed. The monthly average two-meter temperature and total precipitation anomalies are the target variables that the AI models are asked to reconstruct.

Note that we intentionally do not detrend the two-meter temperature data, allowing the AI model to potentially capture the anthropogenic trend.

3.4 | SEAS5 bias-corrected forecast

Bias correction is a crucial step in calibrating the forecast by removing systematic biases. The distribution of simulated climate variables is adjusted to better match the observed historical data by mapping the quantiles of the model output to those of the reference dataset, ensuring that biases in the mean, variance, and higher-order statistical properties are minimized. Empirical quantile mapping (EQM) is a widely employed method for bias-correcting the forecast data (Crespi et al., 2021; Ratri et al., 2021; Golian and Murphy, 2022). We apply the EQM to bias-correct monthly aggregated Z500, two-meter temperature, and precipitation for each of the 25 ensemble members and each of the seven forecasting lead times separately. To perform the EQM we use the python package `xclim` (Bourgault et al., 2023). The hindcast period, spanning the months from January 1981 to December 2010, is used to bias-correct the SEAS5 forecasts from January 2011 to December 2024, using ERA5 data upscaled to $1^\circ \times 1^\circ$ resolution as reference. Note that the hindcast period used for the bias correction coincides with the climatological period.

The calendar day climatology and standard deviation of Z500, two-meter temperature and precipitation, derived from ERA5 data (see steps 1 to 5 in Sec. 3.1), are ag-

gregated to monthly values to obtain the SEAS5 monthly anomalies for these variables. Explicitly, the monthly average of the calendar day climatology (steps 1 to 4) is subtracted from the SEAS5 bias-corrected monthly forecasts. The resulting anomalies are then divided by the monthly average of the standard deviation computed in step 5.

Despite the AI models are trained on the I_{wr} computed from ERA5 Z500 standardized anomalies, $\tilde{\Phi}(r, \lambda, \phi)$, it is interesting to evaluate its performance in reconstructing the monthly average two-meter temperature and total precipitation anomalies using the predicted I_{wr} computed from the bias-corrected SEAS5 Z500 forecast, I_{wr}^{SEAS5} . To obtain I_{wr}^{SEAS5} we project the forecast of the bias-corrected monthly mean Z500 standardized anomalies for each ensemble member m and lead-time month l , $\tilde{\Phi}^{SEAS5}(t, \lambda, \phi, l, n)$, to the seven mean cluster centers computed from the ERA5 daily anomalies, $\tilde{\Phi}_{wr}(\lambda, \phi)$, (see Sec. 3.1). The calculations follow closely Eqs. 1 and 2, with the additional dimensions l and m .

4 | AI-MODEL

The AI models are designed to reconstruct the monthly average of the standardized two-meter temperature and total precipitation anomalies in Europe (Sec. 3.3) from the monthly average WR index, I_{wr} (Sec. 3.1).

4.1 | Models' architecture and training

Fig. 2 schematically describes the models' architecture. The monthly average I_{wr} , for each WR, is passed along with the corresponding encoded month and year as input to the models. The month is encoded in twelve categories using one-hot encoding. One-hot encoding is a widely used technique in machine learning and data processing for representing categorical variables as numerical vectors. In our scenario, we encode the month = 1,...,12, into a twelve-dimensional vector, e.g., January (month = 1) is encoded in (1,0,...,0); February (month = 2) is encoded in (0,1,0, ...,0). The inputs are then processed first by a linear layer and subsequently

by a sequence of two ResNet blocks. ResNet (Residual Network) introduces shortcut connections, allowing the model to learn residual mappings instead of direct transformations, which makes it easier to train deep architectures. The use of ResNet blocks helps mitigate the vanishing gradient problem, ensuring stable and efficient training of deeper networks, which is particularly beneficial when working with limited data. The ResNet blocks take the 20-dimensional input (seven WR, the year, and the twelve-dimensional encoded month) and yield a vector of $N = 28$ dimensions. Expanding the feature space is a common strategy in NN, as it enables the model to better capture and process the information in the input data by learning a more expressive representation of the temporal predictors. The N -dimensional vector is stacked pixel-by-pixel with the two-dimensional static data: the latitude grid, the longitude grid, the land-sea mask, and the digital terrain model (DTM) of the European region with the same resolution as the output two-dimensional field. Stacking these features pixel-by-pixel with the static spatial data enables the model to condition its reconstructions on both large-scale atmospheric drivers and local geographical features. The resulting $(N + 4) \times n_\lambda \times n_\phi$ tensor, where n_ϕ and n_λ are the numbers of latitude and longitude grid points, respectively, is the input of the following convolutional ResNet blocks, which reduce the number of features to one, i.e., to a two-dimensional field representing the target anomalies. Convolutional layers capture both local spatial patterns and cross-grid dependencies, enabling the model to learn large-scale drivers and their geographically-modulated regional responses. We use 3x3 kernels in all the convolutional layers. These layers combine the information encoded in the feature vector with the static spatial data by selecting the components of the feature vector most relevant to each grid point. A 3x3 kernel is sufficiently small to capture local structure. We noticed that increasing the number of convolutional ResNet layers did not improve the performance of the model. We employ ReLU activation functions to introduce non-linearity in a computationally efficient way, enabling the model to capture complex patterns.

The AI models are trained separately to reconstruct

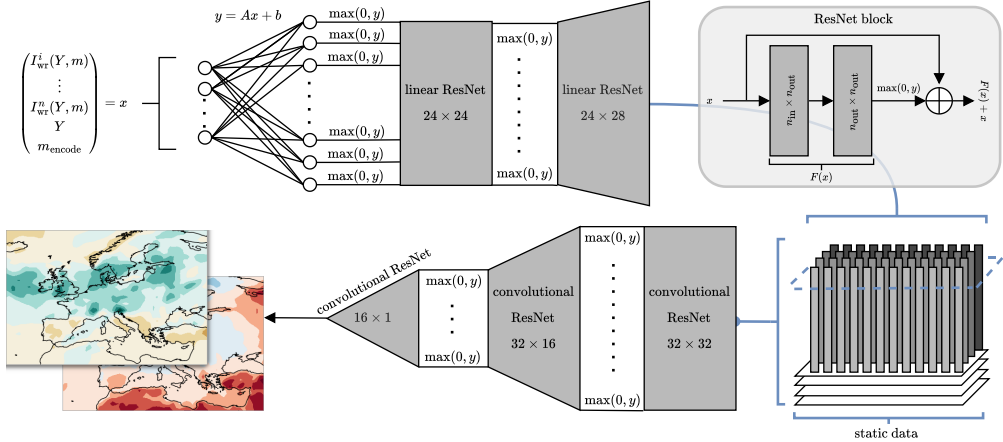


FIGURE 2 Schematic representation of the model's architecture. The input vector x , which includes the n WR indices, the year, and the encoded month, is passed as input to the model. After each layer, the output y is passed to a ReLU activation function $\max(0, y)$. The $N = 28$ dimensional vector, output of the second linear ResNet block, is stacked pixel-by-pixel onto the static data (latitude and longitude grids, land-sea mask, and digital terrain model). The resulting $(N + 4) \times n_\lambda \times n_\phi$ tensor, where n_ϕ and n_λ are the number of latitude and longitude grid points, respectively, is the input of the first convolutional ResNet layer. The number of features is then reduced by two by the second ResNet block and to one (temperature or precipitation field) by the final ResNet layer

two-meter temperature and total precipitation anomalies. They learn to approximate the target anomalies by adjusting their internal $\approx 30k$ parameters to minimize the training loss between the predicted and observed anomaly fields. We choose the mean squared error (MSE) as training loss, defined in Sec. 4.2. For more details about the training setup and hyperparameters, the reader can refer to Appendix C. To properly assess models' performance and their generalization ability, the dataset is divided into distinct training, validation, and test periods. The training set spans from January 1940 to December 2005. The months from January 2006 to December 2010 are used to avoid overfitting, by halting the training when the validation MSE reaches a minimum. To finally assess the performance of the model, the remaining months from January 2011 to December 2024 are used. Note that the climatology period, used to compute the anomalies of the WR, does not include the test dataset.

The models' performance can be slightly influenced

by the order in which the input and output pairs of the train dataset are passed to the models during training. We use random ordering and repeat the training procedure six times to account for the dependence of the model's performance on the training data random ordering.

The limited size of the training dataset (65 years) constrains the choice of models' architecture, preventing the use of larger and more complex architectures. Such architectures, with their higher number of parameters, would not only be computationally inefficient but also more prone to overfitting in data-scarce settings.

4.2 | Evaluation metrics

After performing an average on the six reconstructed anomalies by each of the six trained models, the quality of the reconstructed fields is evaluated using the metrics described in the following paragraphs.

Mean Absolute Error (MAE)

Is a commonly used metric to evaluate the accuracy of a model in predicting numerical values. It measures the average magnitude of errors by considering the absolute differences between actual and predicted values. Given a dataset with n observations, where y_i represents the actual values and \hat{y}_i the predicted ones, MAE is computed as

$$\text{MAE} = \frac{1}{n} \sum_{i=1}^n |y_i - \hat{y}_i|. \quad (3)$$

A lower MAE indicates a more accurate model. Since it relies on absolute differences, it treats overestimation and underestimation equally.

Anomaly Correlation Coefficient (ACC)

ACC is a statistical measure to assess the similarity between predicted and observed anomalies in a dataset. It is commonly applied in climate science to evaluate the accuracy of deterministic forecasts. ACC quantifies how well the anomalies correlate between predictions and observations. Given a set of anomalies for n observations, where y_i represents the observed anomalies and \hat{y}_i the predicted ones, anomaly correlation coefficient (ACC) is computed as

$$\text{ACC} = \frac{\sum_{i=1}^n (y_i - \bar{y})(\hat{y}_i - \bar{\hat{y}})}{\sqrt{\sum_{i=1}^n (y_i - \bar{y})^2} \sqrt{\sum_{i=1}^n (\hat{y}_i - \bar{\hat{y}})^2}}, \quad (4)$$

where \bar{y} and $\bar{\hat{y}}$ denote the mean values of observed and predicted anomalies, respectively. The ACC ranges from -1 to 1 , with values close to 1 indicating a strong positive correlation, meaning that the model effectively captures the variations in anomalies. Conversely, values near 0 suggest no correlation, while negative values indicate an inverse relationship between predicted and observed anomalies.

To assess whether an observed correlation is statistically significant, we compute the associated two-tailed p-value, derived from the exact distribution of the sample correlation coefficient, which follows a scaled beta distribution. The two-tailed p-value represents the probability of obtaining a higher or equal correlation assuming that

there is no actual correlation (i.e., under the null hypothesis of zero correlation). In this context, a p-value below 0.05 is typically considered statistically significant, indicating that there is less than a 5% probability that the observed correlation occurred by chance. Thus, correlations with $p < 0.05$ can be interpreted as significant at the 95% confidence level.

Coefficient of efficiency (CE)

CE is a statistical measure used to evaluate the predictive skill of a model by comparing its performance to that of a validation climatology (Bürger, 2007), thus indicating the shared variance between the observed and estimated data throughout the verification period. Given n observations, where y_i represents the actual values, \hat{y}_i the predicted values, and \bar{y} the mean of observed values, the coefficient of efficiency (CE) is computed for each grid point as,

$$\text{CE} = 1 - \frac{\sum_{i=1}^n (y_i - \hat{y}_i)^2}{\sum_{i=1}^n (y_i - \bar{y})^2}. \quad (5)$$

A value of $\text{CE} = 1$ indicates a perfect prediction, while $\text{CE} = 0$ suggests that the model performs no better than the validation climatology. Negative values imply that the model performs worse than the reference. In this study, we use the climatology of the 2011 – 2024 testing period as validation climatology. When the CE is evaluated during a specific season, only the related months are used to compute the validation climatology.

Since CE is not bounded from below, it is possible to have negative outliers in its distribution. We then prefer to use medians instead of averages when aggregating the skills discussed in this paragraph to avoid the outliers from significantly imbalancing the results.

To evaluate the aforementioned deterministic metrics on SEAS5, unless otherwise specified, we use the ensemble mean as the predicted value.

Continuous Ranked Probability Score (CRPS)

CRPS is a widely used proper scoring rule for ensemble predictions (Hersbach, 2000). The continuous ranked probability score (CRPS) measures the integrated squared difference between the cumulative distribution function (CDF) of the forecast ensemble, F , and the empirical CDF of the verifying observation, $H(\hat{y}) = 1_{\{\hat{y} \geq y\}}$, where y is the observed value. Formally, the CRPS is defined as

$$\text{CRPS}(F, y) = \int_{-\infty}^{\infty} [F(\hat{y}) - H(\hat{y} - y)]^2 d\hat{y}, \quad (6)$$

which reduces to the mean absolute error (MAE) in the case of deterministic forecasts. Unlike the MAE, the CRPS accounts for the full ensemble distribution. Lower CRPS values indicate higher forecast skill, with a score of zero corresponding to a perfect forecast.

In practice, when the forecast distribution is represented by a finite ensemble $\{f_1, f_2, \dots, f_m\}$ of size m , the CRPS can be approximated by

$$\text{CRPS}(F, y) \approx \frac{1}{m} \sum_{i=1}^m |f_i - y| - \frac{1}{2m^2} \sum_{i=1}^m \sum_{j=1}^m |f_i - f_j|. \quad (7)$$

The first term represents the mean absolute error of the ensemble members with respect to the observation, while the second term is a correction for the internal spread of the ensemble.

Spread–Skill Ratio (SSR)

The relationship between ensemble spread and forecast error is commonly assessed using the spread–skill ratio (SSR). For an ensemble of size m with mean forecast \bar{y}_t at time t and verifying observation y_t , the ensemble spread is defined as

$$\sigma_t = \sqrt{\frac{1}{m-1} \sum_{i=1}^m (\hat{y}_{i,t} - \bar{y}_t)^2}, \quad (8)$$

while the forecast error of the ensemble mean is measured by the root-mean-square error (RMSE),

$$\text{RMSE} = \sqrt{\frac{1}{T} \sum_{t=1}^T (\bar{y}_t - y_t)^2}. \quad (9)$$

The SSR is then given by the ratio between the temporal mean of the spread and the RMSE,

$$\text{SSR} = \frac{\bar{\sigma}_t}{\text{RMSE}}. \quad (10)$$

An ideal ensemble forecast is characterized by $\text{SSR} \approx 1$, indicating that the predicted spread reliably reflects the actual forecast uncertainty. Values of $\text{SSR} < 1$ denote an under-dispersive and overconfident ensemble, in which the spread underestimates the true forecast error, whereas $\text{SSR} > 1$ indicates over-dispersion, with the ensemble spread being too large relative to the error.

5 | RESULTS

In the following sections, we evaluate the performance of the AI models in reconstructing monthly mean two-meter temperature and total precipitation anomalies in winter (DJF) and summer (JJA) from January 2011 to December 2024. Sec. 5.1 presents the spatial reconstruction of these anomalies by the AI models trained with the seven year-round WR indices. We compare the performance of the AI model with the most commonly used reconstruction methods in Sec. 5.2. We further investigate the skill of the models with respect to: (a) the number of WR indices used for training and as input (Sec. 5.3); (b) the impact of errors on I_{wr} on the reconstruction (Sec. 5.4); and (c) the use of I_{wr}^{SEAS5} as input (Sec. 5.5). The first two aspects address how the reconstruction quality degrades, identifying a threshold to achieve a better seasonal forecast than SEAS5. The third point examines the accuracy of the reconstructed anomalies when using WR indices predicted by SEAS5. It can be interpreted as a hybrid NWP-AI framework for forecasting European mean two-meter temperature and total precipitation in winter and summer.

Although the AI models reconstruct the anomalies over the entire European region as defined in Sec. 3.3, in the following analysis, we restrict the evaluation to land areas only.

5.1 | Anomaly reconstruction with seven WR

A qualitative comparison between the reconstructed monthly mean two-meter temperature (left column) and total precipitation (right column) against ERA5 is shown in Fig. 3. The first row presents the best reconstruction, while the second row illustrates the worst reconstruction. Best and worst reconstructions are identified by the minimum and maximum MSE on the test set, respectively, evaluated after training. In the best-case scenario, the AI model is able to capture part of the spatial distribution of monthly two-meter temperature and total precipitation anomalies. However, it generally fails to reproduce extremes and more localized patterns, resulting in reduced spatial variability compared to the reanalysis. The worst-case scenarios usually occur when ERA5 anomalies are particularly strong. In such cases, the MSE increases if the model does not adequately reproduce either the magnitude or the spatial distribution of the anomalies. A representative example is the monthly total precipitation: while the model successfully mimics the spatial distribution in parts of Central Europe, as well as the Iberian and Scandinavian Peninsulas, it underestimates the magnitude of the extremes, which in this case reach up to 20 cm. The underestimation of extremes is a common issue for many NN architectures trained using the MSE.

Fig. 4 shows the spatial MAE, ACC and CE in reconstructing the European monthly mean two-meter temperature and total precipitation anomaly using the seven year-round WR indices, I_{wr} , in the winters and summers during the test years.

For the two-meter temperature anomaly, the MAE maps indicate low reconstruction errors across most of Europe, especially in western, central, and southern regions, with values frequently below 1.5K. Errors are slightly higher in northern and eastern areas, particularly during winter, which is related to the higher variability and amplitude of the two-meter temperature anomalies in those regions, as demonstrated by the higher standard deviation (not shown). The ACC maps show high correlations (generally above 0.5) between reconstructed and

observed anomalies, particularly over western, central, and southern Europe in both winter and summer, as well as in some parts of Northern Europe. This indicates the model effectively captures temporal variability in these areas. The CE metric partially mirrors this pattern, with values approaching 0.3 in winter, signifying that the model performs appreciably better than a climatological reference. In summer, the CE remains low but generally above zero.

In the case of precipitation, the MAE values are more spatially variable and generally higher than for temperature. Nonetheless, several regions, especially parts of Eastern and Northern Europe, exhibit relatively low MAE, particularly in winter. The ACC values for precipitation in winter are generally above 0.5 across most regions of Europe, except for some areas in central and eastern Europe. In the summer season, the ACC values remain positive but are generally low, with large regions falling below 0.5 and correlations that are not statistically significant ($p > 0.05$). During this season, the AI model driven by the WR indices is largely unable to capture precipitation trends accurately, except in some regions of northern Europe. CE values for precipitation exhibit a similar spatial pattern of ACC, with positive skill in central Europe and part of Scandinavia during winter but a marked decline in the central and eastern regions during summer.

Summer extratropical variability is less influenced by the large amplitude stationary waves and tropical forcing that characterize the boreal winter climate. As a result, the summer weather in the Northern Hemisphere is more influenced by regional-scale processes, such as mesoscale convective weather systems and land-atmosphere coupling (Ambrizzi et al., 1995; Koster et al., 2000; Schubert et al., 2011). This explains the lower skill reached by the AI models in summer compared to winter in all the skills tested. In particular, summer CE reveals that models using the Euro-Atlantic WR are unable to accurately reconstruct the mean two-meter temperature and total precipitation anomalies in the Mediterranean and Black Sea regions. For these areas, the reconstruction could be improved by incorporating the Mediterranean large-scale circulation (Mastrantonas et al., 2021) and including other predictors, such as soil

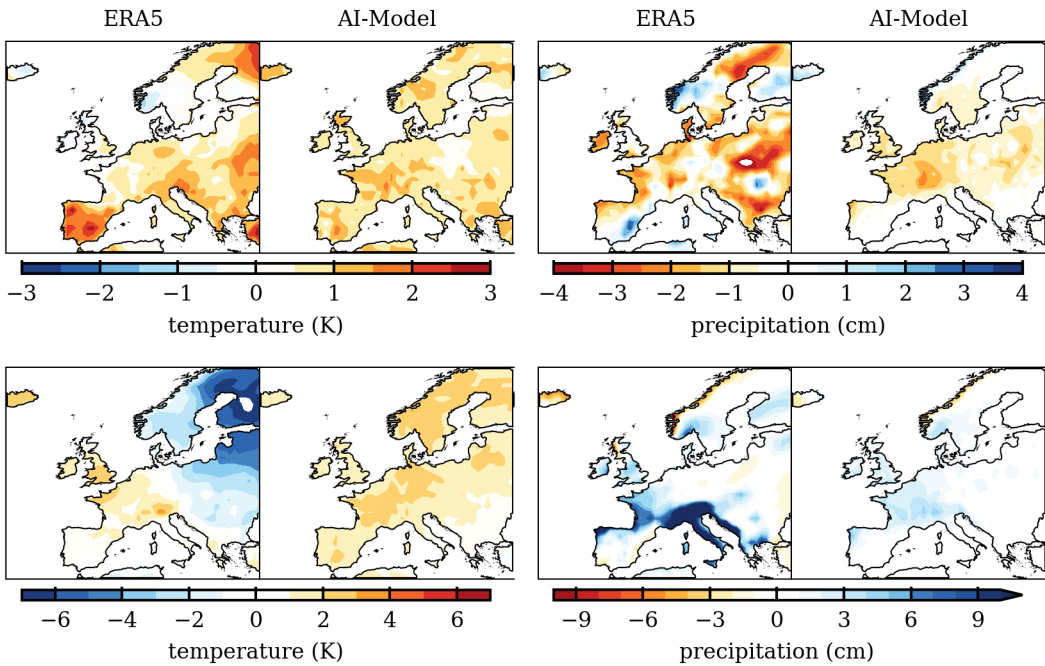


FIGURE 3 Qualitative comparison of reconstructed monthly mean two-meter temperature (left column) and total precipitation (right column) against ERA5. The top row displays the cases with the lowest mean squared error, while the bottom row shows those with the highest. The best (worst) reconstruction for temperature corresponds to July 2016 (February 2011), while for precipitation it is August 2013 (November 2019).

moisture or rainfall deficit indices (Vautard et al., 2007). In fact, the authors of the latter study demonstrate that “hot summers are preceded by winter rainfall deficits over Southern Europe”. Including indices that capture rainfall deficits (e.g., the Standardized Precipitation Index, SPI) and/or soil moisture (e.g., the Soil Moisture Deficit Index, SMDI) from the preceding season could enhance the reconstruction of the Southern European climate. We hypothesize that our model would be capable of capturing the relationship between these indices and the monthly summer anomalies of two-meter temperature and total precipitation in the region.

5.2 | Comparison with regressions on individual WR

We compare the performance of the AI models against a benchmark based on monthly composites of tempera-

ture and precipitation for each of the seven WR (see, e.g., Grams et al., 2017; Madonna et al., 2021; Gerighausen et al., 2024). We first identify the dominant WR for each month in the winters and summers from 1981 to 2010. A WR is considered dominant if its *monthly* index exceeds all other WR indices and is larger than its standard deviation over the climatology. We then compute the typical monthly two-meter temperature and total precipitation associated with each WR by averaging the respective values over all months in which that WR was dominant. Months without a clearly dominant WR are assigned to a “no-regime” composite. Since each WR can have a different impact on the ground variables depending on the season, the average is computed separately for the months in the winter (DJF) and summer (JJA) season. For the reconstruction period (2011 onward), we assign to each month the composite corresponding to its active dominant WR, or the no-regime composite if no dominant WR could be

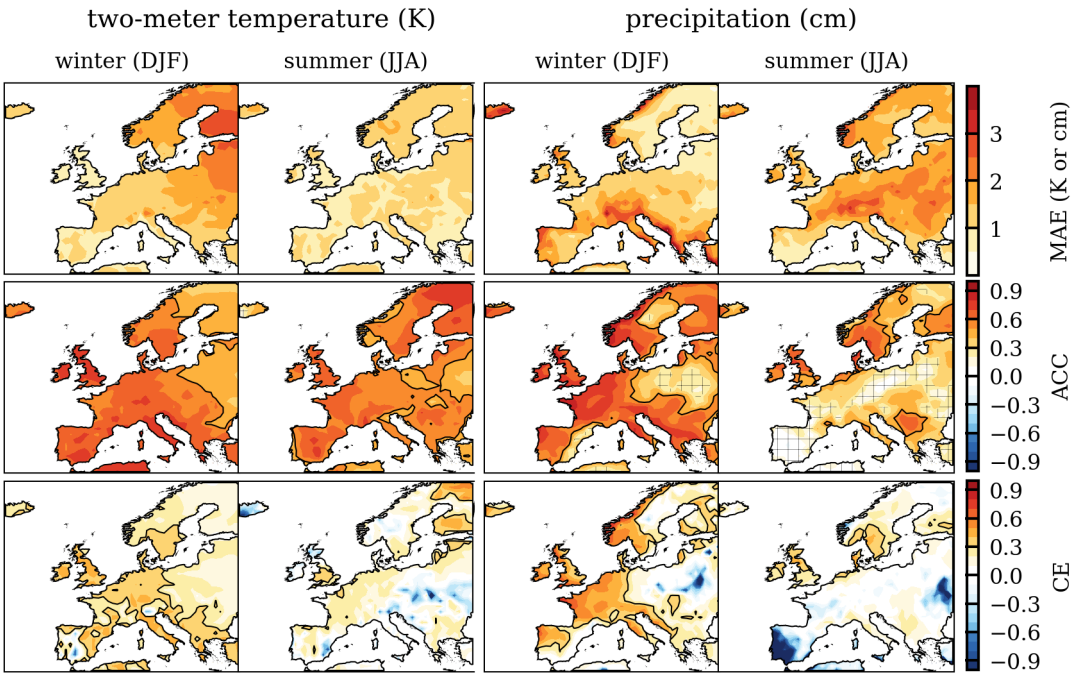


FIGURE 4 AI models spatial MAE (top), ACC (middle) and CE (bottom) in reconstructing the winters (first and third columns) and summers (second and fourth columns) mean two-meter temperature and total precipitation anomalies using seven WR indices in the test years (from January 2011 to 2024). Hatched areas mark regions with correlations that are not significant at $p > 0.05$. Black contours indicate regions with ACC (CE) higher than 0.5 (0.3).

identified, applying the same classification used in the climatology. As for the AI model, this approach relies on monthly average indices as predictors, enabling a direct comparison.

The composite reconstructions are evaluated using the deterministic metrics introduced in 4.2 against ERA5 monthly data. Relative scores are computed with respect to the AI-model as:

- relative improvement of the MAE: $(\text{Composite MAE} - \text{AI-Model MAE}) / \text{Composite MAE}$,
- relative improvement of the ACC: $(\text{AI-Model ACC} - \text{Composite ACC}) / (1 - \text{Composite ACC})$,
- relative improvement of the CE: $(\text{AI-Model CE} - \text{Composite CE}) / (1 - \text{Composite CE})$.

These scores highlight the relative improvement of the AI model with respect to the regressions on individual

WR as a benchmark.

Fig. 5 shows the relative improvement in percentage for both the two-meter temperature and total precipitation reconstruction in winter and summer from 2011 to 2024. The AI models outperform the simple composite benchmark across all seasons, variables, and metrics, with only a few regional exceptions. The improvement is particularly relevant for ACC and CE of the two-meter temperature reconstruction in central and Mediterranean Europe for both seasons, and particularly during summer, with the exception of some areas in Norway, Sweden, Greenland, and the British Isles. Also, the ACC and CE of the total precipitation show substantial improvements in many areas, but with less spatial consistency and with few regions characterized by negative scores in the Iberian peninsula.

Overall, the comparison demonstrates that while the composite method provides a simple and interpretable

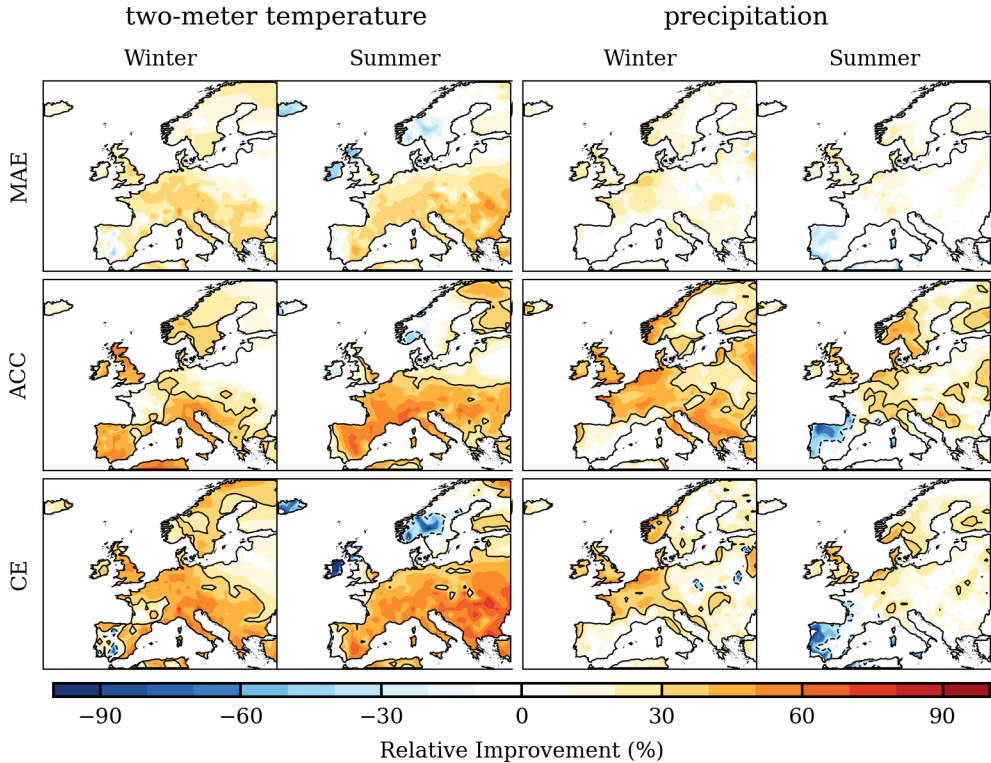


FIGURE 5 Relative improvement of the AI models with respect to the regressions on individual WR as benchmark. First (second) [third] row shows the relative improvement in MAE (ACC) [CE] for both two-meter temperature and total precipitation separately for the winter (December, January, February) and summer (June, July, August) from 2011 to 2024. Solid (dashed) contours indicate regions with relative improvement higher (lower) than 30%.

benchmark, the AI models are capable of capturing subtle combinations of WR patterns and reproducing regional variability more accurately. These results highlight the added value of data-driven reconstructions over traditional composite approaches, particularly when the underlying regime dynamics are complex.

5.3 | Impact of the number of WR on the reconstruction

In Fig. 6, the reconstruction skills (MAE, ACC, and CE) of the AI models for monthly mean two-meter temperature and total precipitation anomalies during winter (DJF) and summer (JJA) are compared across configurations using

seven WR indices (red), four WR indices (orange), the NAO index (light blue), and no indices (blue) as input. Analogously, Tab. 1 and Tab. 2 report the medians of the same metrics and the uncertainties on the last significant digit reported in parentheses. The uncertainties are computed as the semi-difference of the skill metrics' medians across multiple model initializations with different random seeds, to quantify the spread due to the random seed initialization. The models trained without indices (No index) consistently show the lowest scores for both temperature and precipitation. Despite this, the model retains limited skill for two-meter temperature, with median ACC around 0.28 ± 0.03 in winter and 0.32 ± 0.03 in summer. This likely results from the AI

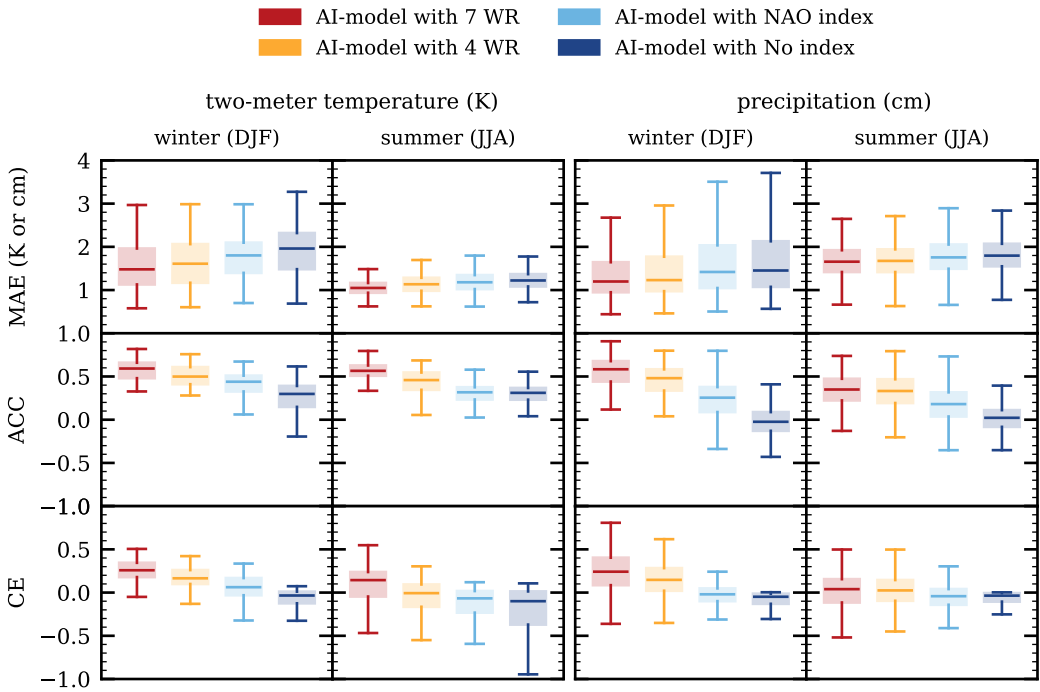


FIGURE 6 2011 – 2024 winters (first and third columns) and summers (second and fourth columns) MAE (top row), ACC (middle row) and CE (bottom row) of the two-meter temperature anomalies and precipitation anomalies, reconstructed by the AI models trained with seven WR (red), four WR (orange), NAO (light-blue) and zero (blue) indices. The box plots summarize the spatial data, showing the median (central line), interquartile range (box), and range.

model capturing the long-term climate trend through the year and month inputs. However, the spatial distribution of this correlation lacks statistical significance in large regions, as shown in Fig. D.1. The inclusion of the NAO index leads to some improvements. Since the NAO alone explains approximately 25% (16 %) of the atmospheric circulation variance in winter (summer), it significantly enhances the ACC for both variables in winter. Interestingly, for temperature in summer, the skills are comparable between the models using the NAO index and without indices. We speculate that much of the reconstruction skill for the summer temperature likely arises from anthropogenic trends, with only a comparatively small contribution from the NAO. A thorough assessment of this hypothesis is beyond the scope of the present work. The reconstruction of summer precipitation has

instead a general improvement with respect to the model trained without indices. Training the models with four WR indices yields substantial gains over the NAO models across both seasons and variables. For temperature, the typical improvements in ACC are about 28% in winter and 16% in summer, while for precipitation, they reach 74% (DJF) and 100% (JJA). The CE also improves, particularly for the winter season. Although CE remains near zero or slightly negative in summer, the four-index models exhibit far more dynamical skill and robustness than models with fewer indices. Expanding to seven WR indices results in reduced yet consistent improvements. The MAE remains largely comparable to the four WR setup, while ACC increases by 27% (DJF) and 35% (JJA) for temperature and by 17% (DJF) and 14% (JJA) for precipitation. The CE improves by approximately 113%

Two-meter temperature					
Season	Metric	7 WR	4 WR	NAO	No idx
	MAE (K)	0.78(3)	0.91(5)	1.04(6)	1.01(2)
DJF	ACC	0.65(4)	0.51(1)	0.40(2)	0.28(3)
	CE	0.32(7)	0.15(2)	-0.01(4)	-0.04(1)
	MAE (K)	0.77(2)	0.88(6)	0.93(3)	0.82(2)
JJA	ACC	0.50(5)	0.37(3)	0.32(1)	0.32(3)
	CE	0.07(5)	-0.03(6)	-0.09(3)	-0.08(2)

TABLE 1 Median MAE, ACC, and CE for monthly mean two-meter temperature in DJF and JJA using seven WR, four WR, NAO, or no index as AI model input. Uncertainties on the last significant digit (in parentheses) denote the semi-difference (half the difference between maximum and minimum) of the skill metrics' medians across multiple model initializations with different random seeds.

Total precipitation					
Season	Metric	7 WR	4 WR	NAO	No idx
	MAE (cm)	1.34(1)	1.41(3)	1.66(2)	1.86(1)
DJF	ACC	0.63(1)	0.54(2)	0.31(2)	-0.02(2)
	CE	0.32(2)	0.22(2)	0.01(2)	-0.05(1)
	MAE (cm)	1.29(1)	1.25(2)	1.32(1)	1.45(1)
JJA	ACC	0.39(1)	0.34(3)	0.17(1)	0.00(2)
	CE	0.07(1)	0.03(2)	-0.04(1)	-0.04(1)

TABLE 2 As Tab. 1 but for monthly mean total precipitation in DJF and JJA using seven WR, four WR, NAO, or no index as AI model input. Uncertainties on the last significant digit (in parentheses) denote the semi-difference (half the difference between maximum and minimum) of the skill metrics' medians across multiple model initializations with different random seeds.

for temperature and 45% for precipitation in winter, but remains low in summer.

In view of a data-driven forecast of WR indices followed by the anomalies reconstruction, we suggest that using at least four WR indices can provide an effective balance between reconstruction performance and index predictability, offering robust and meaningful reconstruction skills for both temperature and precipitation in winter and summer.

5.4 | Reconstruction degradation with index errors

The 50 perturbed indices for each value of the perturbation MARE are used as input to the AI models. The MAE, the ACC, and the CE for the summer and winter seasons can be evaluated as usual for each of the 50 reconstructed variables. After the skills are computed for each realization, we perform an average over the random realizations to evaluate the skills for the given MARE.

The spatial median of the mean two-meter temperature and total precipitation ACC and CE, averaged over the 50 random realizations of the perturbed indices,

are shown in Fig. 7 for the 2011 – 2024 winters and summers. Increasing the MARE of the perturbed indices, the AI models' skills naturally degrade up to a point where they can be worse than the SEAS5 ensemble-mean ACC and CE. Both in winter and summer, the median ACC of the reconstructed mean two-meter temperature and total precipitation is always better than the SEAS5 ensemble-mean forecast ACC, indicating a strong efficacy of the AI models in capture the correlation between the Euro-Atlantic WR and European two-meter temperature and precipitation also in the presence of Gaussian distributed errors on the input indices. As for the ACC, the median CE of the mean two-meter temperature in winter and the precipitation in summer is always higher than the respective SEAS5 ensemble-mean median CE. More interesting is the case of the median CE of the reconstructed total precipitation and mean two-meter temperature, which becomes comparable to the relative SEAS5 skill at MARE = 100%. Taking the lower value of MARE of 80% as a reference, this poses a lower bound on the forecast accuracy of the seven I_{wr} required to have a seasonal forecast of the mean two-meter temperature and total precipitation

with higher deterministic skills than the bias-corrected SEAS5 ensemble mean forecast used in this work. We can express the results obtained here in terms of MAE of the perturbed indices, $\langle |I_{wr} - I'_{wr}| \rangle = 0.35$ for MARE of 80%.

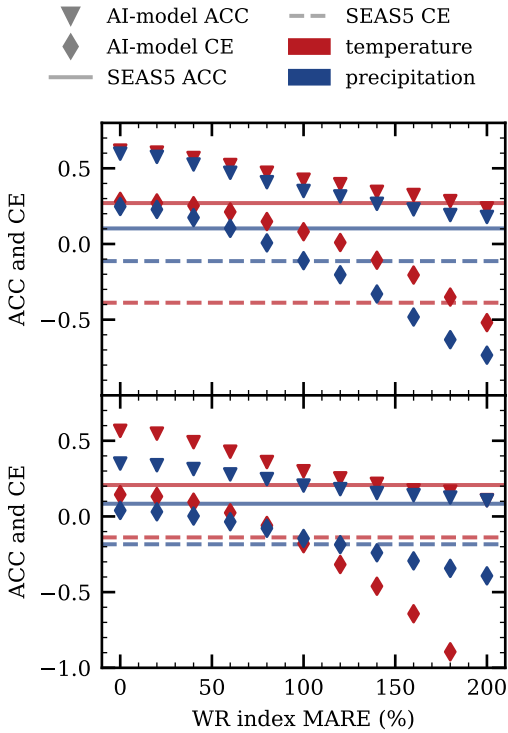


FIGURE 7 Spatial median of the mean two-meter temperature (red) and total precipitation (blue) ACC (triangles) and CE (rhomboids) reconstructed by the AI models in the winter seasons (top panel) and summers (bottom panel) from 2011 to 2024, as a function of index MARE. The values are averaged over 50 random realizations of I'_{wr} sampled from $I_{wr} \times N(0, \sqrt{\pi/2} \text{MARE})$. Horizontal lines are the SEAS5 spatial median of the ACC (solid) and CE (dashed) for the same variables and seasons.

5.5 | AI-models in a concrete forecasting scenario

To test the AI models in a real forecasting scenario, we now analyze the reconstruction of the monthly mean

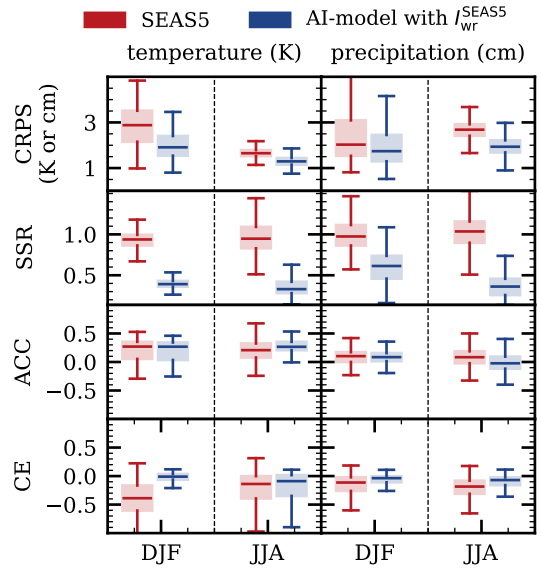


FIGURE 8 CRPS (first row), SSR (second row), ACC (third row) and CE (last row) for the SEAS5 (red) and the AI models using I_{wr}^{SEAS5} as input (blue). The first and second columns show the winter (left half) and summer (right half) skills for the two-meter temperature and precipitation, respectively. The box plots summarize the spatial data, showing the median (central line), interquartile range (box), and range.

two-meter temperature and total precipitation when using the monthly mean seven WR indices forecasted by the bias-corrected SEAS5, I_{wr}^{SEAS5} (see Sec. 2.2), as model inputs. Although the AI models are not inherently designed for ensemble forecasting, since they are trained deterministically using the MSE loss, an ensemble can nevertheless be constructed by driving the models with the seven I_{wr}^{SEAS5} forecasts from each SEAS5 ensemble member. This allows us to evaluate not only deterministic metrics based on the ensemble means, but also probabilistic scores such as the CRPS and the SSR for both the hybrid NWP-AI models and SEAS5. In the following, the SEAS5 forecasts for the winters (summers) are initialized on the first of November (May) to predict December, January, and February (June, July, and August).

Fig. 8 presents a comparative assessment of the hybrid NWP-AI models and the SEAS5 forecasting system

for boreal winter and summer. The NWP-AI models typically exhibit better or comparable skills to the SEAS5 forecast. In particular, they achieve lower CRPS values, particularly for the winter mean two-meter temperature and summer total precipitation anomalies. This enhanced performance is likely attributable to the use of an MSE loss during training, which suppresses variability in the models' output. In contrast, SEAS5 tends to produce forecasts with higher variability, often resulting in higher MAE but with an SSR near the unity. The overconfidence of the hybrid NWP-AI approach is its major drawback: the ensemble spread is markedly reduced by the AI model, which is not adequately designed and trained to face a probabilistic forecast. In the conclusions, we outline possible directions for addressing this limitation. The reduced MAE of the NWP-AI models translates into higher values of the CE, especially in cases where the discrepancy in MAE relative to SEAS5 is substantial. Nevertheless, both SEAS5 and NWP-AI models yield CE values that are often close to or below zero, indicating limited skill relative to the climatology of the test dataset. Regarding the ACC, the NWP-AI models slightly outperform SEAS5 for the two-meter temperature in both seasons. For the total precipitation anomalies, the ACC is comparable in winter and worse in summer.

Considering the stability of the AT-model in the presence of Gaussian-distributed errors in the WR indices, as discussed in Sec. 5.4, the relatively poor performance of the NWP-AI models compared to the AI model driven by perfect indices indicates that the SEAS5 forecast of the WR (i.e., $Z500$) has limited skill. Indeed, the CRPS of the indices degrades rapidly with forecast lead time, reaching around 0.6 already for forecasts of the month following the initialization (see Appendix E).

6 | CONCLUSIONS

This study presents and evaluates two lightweight AI based models for reconstructing monthly anomalies of two-meter temperature and total precipitation in Europe using Euro-Atlantic WR indices. The models demonstrate robust skill in capturing both spatial and

temporal variability of temperature, with somewhat reduced performance for precipitation. Reconstruction skills are higher during winter, reflecting the stronger influence of large-scale circulation patterns on surface climate during this season. We test the performance of the models by varying the number of WR indices used as input. Despite the models using seven WR achieving the best skills, four indices represent a reasonable trade-off between reconstruction accuracy and forecast feasibility. We further assess the models' robustness to errors in the input WR indices and identify a lower bound on their forecast accuracy necessary to outperform a state-of-the-art dynamical forecasting system, SEAS5. Specifically, to exceed SEAS5's skill, the indices of winter (DJF) and summer (JJA) must be predicted with an MARE below approximately 80%, corresponding to a MAE of about 0.35 when the indices are normalized by the mean and standard deviation of the 1981 - 2011 climatology. Finally, in a realistic forecasting setup where the WR indices are derived from bias-corrected SEAS5 forecasts, the hybrid NWP-AI models achieve comparable or superior performance relative to SEAS5, particularly for winter temperature and summer precipitation. These results highlight the potential of AI-driven approaches, grounded in dynamical predictors like WR indices, to complement traditional numerical forecasting methods for improved long-range climate prediction.

Nonetheless, several limitations remain. Training AI models usually requires a large amount of data. We use monthly values from 1940 to 2005, totaling 852 points. The small training dataset forces the use of a lightweight architecture with a limited number of trainable parameters. Training with the MSE loss encourages smooth reconstructions with reduced variability. While this leads to lower error scores, it also suppresses part of the natural variability of the climate system. This behavior is typical of a deterministic model trained on pointwise losses, which tend to regress toward the mean state rather than reproduce the full range of plausible outcomes. A natural extension would be to design the architecture for probabilistic reconstruction. For instance, an ensemble of reconstructions could be generated by training the network with proper probabilistic losses such as the CRPS. This

would allow the model to produce a distribution of possible realizations rather than a single deterministic trajectory, better capturing forecast uncertainty and enabling the use of ensemble-based verification metrics.

Despite these limitations, the approach is flexible and adaptable. The model can be extended to other regions, time scales, and surface variables. In particular, the sub-seasonal time scale presents a promising opportunity, offering both a richer dataset and potential for operational forecasting improvements. Recent studies have proposed new approaches for computing the WR (Paepe and Cruz, 2025; Spuler et al., 2024; Springer et al., 2024; Mukhin et al., 2024a). Incorporating these WR could potentially enhance the reconstruction performance of the proposed AI model.

The next efforts will be directed towards a fully probabilistic AI-driven method to forecast the WR indices, which can be used as input to the AI model presented here (or to a probabilistic extension) to obtain a forecast of the surface-level variables.

Acknowledgements

The authors thank Ilaria Tessari and Federico Fabiano for the valuable discussions on the year-round WR calculations. We also thank Leonardo Aragao for the confrontation on the bias-correction of SEAS5. This work was developed with financial support from ICSC–Centro Nazionale di Ricerca in High Performance Computing, Big Data and Quantum Computing, Spoke4 - Earth and Climate, funded by European Union – NextGenerationEU.

Data availability

Daily post-processed ERA5 data on surface (Hersbach et al., 2024b) and pressure levels (Hersbach et al., 2023), was generated using Copernicus Climate Change Service information 2020, obtained from the Copernicus Climate Change Service (Hersbach et al., 2024a,b). Neither the European Commission nor ECMWF is responsible for any use that may be made of the Copernicus information or data it contains. The AI models implemented in this work are written in PyTorch Lightning (Falcon et al., 2020)

and released under the MIT License through a GitHub repository (https://github.com/DSIP-FBK/anom_recon) based on the Lightning-Hydra-Template (Yadan, 2019). The repository also contains all the scripts necessary to reproduce the results discussed in the paper (figures and tables). The data used to train the models is available on Zenodo (<https://zenodo.org/records/17276947>).

Author contributions

Alessandro Camilletti: Investigation, Conceptualization, Methodology, Data Curation, Formal Analysis, Software, Validation, Writing – Original Draft. Gabriele Franch: Methodology, Software, Writing – Review & Editing, Resources, Supervision. Elena Tomasi: Supervision, Writing – Review & Editing. Marco Cristoforetti: Funding acquisition, Project administration, Writing – Review & Editing, Supervision. All authors participated in discussions throughout the development of the study and contributed to refining the manuscript. All authors have read and approved the final version of the manuscript.

Conflict of interest

All authors declare that they have no conflicts of interest.

References

- L. Alfieri, P. Burek, E. Dutra, B. Krzeminski, D. Muraro, J. Thielen, and F. Pappenberger. GloFAS – global ensemble streamflow forecasting and flood early warning. *Hydrology and Earth System Sciences*, 17(3):1161–1175, 2013. doi: 10.5194/hess-17-1161-2013. URL <https://hess.copernicus.org/articles/17/1161/2013/>.
- Tércio Ambrizzi, Brian J. Hoskins, and Huang-Hsiung Hsu. Rossby Wave Propagation and Teleconnection Patterns in the Austral Winter. *Journal of the Atmospheric Sciences*, 52(21):3661–3672, November 1995. ISSN 0022-4928, 1520-0469. doi: 10.1175/1520-0469(1995)052<3661:RWPATP>2.0.CO;2. URL https://journals.ametsoc.org/view/journals/atsc/52/21/1520-0469_1995_052_3661_rwpatp_2_0_co_2.xml. Publisher: American Meteorological Society Section: Journal of the Atmospheric Sciences.
- Philine L. Bommer, Marlene Kretschmer, Fiona R. Spuler, Kir-

- ill Bykov, and Marina M.-C. Höhne. Deep Learning Meets Teleconnections: Improving S2S Predictions for European Winter Weather, April 2025. URL <http://arxiv.org/abs/2504.07625>. arXiv:2504.07625 [cs].
- Pascal Bourgault, David Huard, Trevor James Smith, Travis Logan, Abel Aoun, Juliette Lavoie, Eric Dupuis, Gabriel Rondeau-Genesse, Raquel Alegre, Clair Barnes, Alexis Beaupré Laperrière, Sébastien Biner, David Caron, Carsten Ehbrecht, Jeremy Fyke, Tom Keel, Marie-Pier Labonté, Ludwig Lierhammer, Jwen-Fai Low, Jamie Quinn, Philippe Roy, Dougie Squire, Ag Stephens, Maliko Tanguy, and Christopher Whelan. xclim: xarray-based climate data analytics. *Journal of Open Source Software*, 8(85):5415, May 2023. ISSN 2475-9066. doi: 10.21105/joss.05415. URL <https://joss.theoj.org/papers/10.21105/joss.05415>.
- Jonathan J. Buonocore, Parichehr Salimifard, Zeyneb Magavi, and Joseph G. Allen. Inefficient Building Electrification Will Require Massive Buildout of Renewable Energy and Seasonal Energy Storage. *Scientific Reports*, 12(1):11931, July 2022. ISSN 2045-2322. doi: 10.1038/s41598-022-15628-2. URL <https://doi.org/10.1038/s41598-022-15628-2>.
- Dominik Büeler, Laura Ferranti, Linus Magnusson, Julian F. Quinting, and Christian M. Grams. Year-round sub-seasonal forecast skill for Atlantic-European weather regimes. *Quarterly Journal of the Royal Meteorological Society*, 147(741):4283-4309, 2021. ISSN 1477-870X. doi: 10.1002/qj.4178. URL <https://onlinelibrary.wiley.com/doi/abs/10.1002/qj.4178>. _eprint: <https://onlinelibrary.wiley.com/doi/pdf/10.1002/qj.4178>.
- G. Bürger. On the verification of climate reconstructions. *Climate of the Past*, 3(3):397-409, July 2007. ISSN 1814-9324. doi: 10.5194/cp-3-397-2007. URL <https://cp.copernicus.org/articles/3/397/2007/>. Publisher: Copernicus GmbH.
- Andrej Ceglar and Andrea Toreti. Seasonal climate forecast can inform the European agricultural sector well in advance of harvesting. *npj Climate and Atmospheric Science*, 4(1):42, August 2021. ISSN 2397-3722. doi: 10.1038/s41612-021-00198-3. URL <https://doi.org/10.1038/s41612-021-00198-3>.
- Ashesh Chattopadhyay, Pedram Hassanzadeh, and Saba Pasha. Predicting clustered weather patterns: A test case for applications of convolutional neural networks to spatio-temporal climate data. *Scientific Reports*, 10(1):1317, January 2020. ISSN 2045-2322. doi: 10.1038/s41598-020-57897-9. URL <https://www.nature.com/articles/s41598-020-57897-9>. Publisher: Nature Publishing Group.
- Alice Crespi, Marcello Petitta, Paola Marson, Christian Viel, and Lucas Grigis. Verification and Bias Adjustment of ECMWF SEAS5 Seasonal Forecasts over Europe for Climate Service Applications. *Climate*, 9(12):181, December 2021. ISSN 2225-1154. doi: 10.3390/cli9120181. URL <https://www.mdpi.com/2225-1154/9/12/181>. Number: 12 Publisher: Multidisciplinary Digital Publishing Institute.
- D. P. Dee, S. M. Uppala, A. J. Simmons, P. Berrisford, P. Poli, S. Kobayashi, U. Andrae, M. A. Balmaseda, G. Balsamo, P. Bauer, P. Bechtold, A. C. M. Beljaars, L. van de Berg, J. Bidlot, N. Bormann, C. Delsol, R. Dragani, M. Fuentes, A. J. Geer, L. Haimberger, S. B. Healy, H. Hersbach, E. V. Hólm, L. Isaksen, P. Kållberg, M. Köhler, M. Matricardi, A. P. McNally, B. M. Monge-Sanz, J.-J. Morcrette, B.-K. Park, C. Peubey, P. de Rosnay, C. Tavalato, J.-N. Thépaut, and F. Vitart. The ERA-Interim reanalysis: configuration and performance of the data assimilation system. *Quarterly Journal of the Royal Meteorological Society*, 137(656):553-597, 2011. ISSN 1477-870X. doi: 10.1002/qj.828. URL <https://onlinelibrary.wiley.com/doi/abs/10.1002/qj.828>. _eprint: <https://onlinelibrary.wiley.com/doi/pdf/10.1002/qj.828>.
- Clara Deser, James W. Hurrell, and Adam S. Phillips. The role of the North Atlantic Oscillation in European climate projections. *Climate Dynamics*, 49(9):3141-3157, November 2017. ISSN 1432-0894. doi: 10.1007/s00382-016-3502-z. URL <https://doi.org/10.1007/s00382-016-3502-z>.
- Joshua Dorrington, Isla Finney, Tim Palmer, and Antje Weisheimer. Beyond skill scores: exploring sub-seasonal forecast value through a case-study of french month-ahead energy prediction. *Quarterly Journal of the Royal Meteorological Society*, 146(733):3623-3637, 2020. doi: <https://doi.org/10.1002/qj.3863>. URL <https://rmets.onlinelibrary.wiley.com/doi/abs/10.1002/qj.3863>.
- Heba-Allah Ibrahim El-Azab, R. A. Swief, Noha H. El-Amary, and H. K. Temraz. Seasonal forecasting of the hourly electricity demand applying machine and deep learning algorithms impact analysis of different factors. *Scientific Reports*, 15(1):9252, March 2025. ISSN 2045-2322. doi: 10.1038/s41598-025-91878-0. URL <https://doi.org/10.1038/s41598-025-91878-0>.
- William Falcon, Jirka Borovec, Adrian Wälchli, Nic Eggert, Justus Schock, Jeremy Jordan, Nicki Skafte, Ir1dXD, Vadim Bereznjuk, Ethan Harris, Tullie Murrell, Peter Yu, Sebastian Præsius, Travis Addair, Jacob Zhong, Dmitry Lipin,

- So Uchida, Shreyas Bapat, Hendrik Schröter, Boris Dayma, Alexey Karnachev, Akshay Kulkarni, Shunta Komatsu, Martin B. Jean-Baptiste SCHIRATTI, Hadrien Mary, Donal Byrne, Cristobal Eyzaguirre, cinjon, and Anton Bakhtin. Pytorchlightning/pytorch-lightning: 0.7.6 release, May 2020. URL <https://doi.org/10.5281/zenodo.3828935>.
- Steven B. Feldstein. The dynamics of NAO teleconnection pattern growth and decay. *Quarterly Journal of the Royal Meteorological Society*, 129 (589):901–924, 2003. ISSN 1477-870X. doi: 10.1256/qj.02.76. URL <https://onlinelibrary.wiley.com/doi/abs/10.1256/qj.02.76>. _eprint: <https://onlinelibrary.wiley.com/doi/pdf/10.1256/qj.02.76>.
- Laura Ferranti, Susanna Corti, and Martin Janousek. Flow-dependent verification of the ECMWF ensemble over the Euro-Atlantic sector. *Quarterly Journal of the Royal Meteorological Society*, 141 (688):916–924, 2015. ISSN 1477-870X. doi: 10.1002/qj.2411. URL <https://onlinelibrary.wiley.com/doi/abs/10.1002/qj.2411>. _eprint: <https://onlinelibrary.wiley.com/doi/pdf/10.1002/qj.2411>.
- Laura Ferranti, Linus Magnusson, Frédéric Vitart, and David S. Richardson. How far in advance can we predict changes in large-scale flow leading to severe cold conditions over Europe? *Quarterly Journal of the Royal Meteorological Society*, 144(715):1788–1802, 2018. ISSN 1477-870X. doi: 10.1002/qj.3341. URL <https://onlinelibrary.wiley.com/doi/abs/10.1002/qj.3341>. _eprint: <https://onlinelibrary.wiley.com/doi/pdf/10.1002/qj.3341>.
- Judith Gerighausen, Joshua Dorrington, Marisol Osman, and Christian M. Grams. Quantifying intra-regime weather variability for energy applications, August 2024. URL <http://arxiv.org/abs/2408.04302>. arXiv:2408.04302 [physics].
- Saeed Golian and Conor Murphy. Evaluating Bias-Correction Methods for Seasonal Dynamical Precipitation Forecasts. *Journal of Hydrometeorology*, August 2022. doi: 10.1175/JHM-D-22-0049.1. URL <https://journals.ametsoc.org/view/journals/hydr/23/8/JHM-D-22-0049.1.xml>. Section: Journal of Hydrometeorology.
- Christian Grams, Laura Ferranti, and Linus Magnusson. How to make use of weather regimes in extended-range predictions for Europe. *Publisher: ECMWF*, 2020. doi: 10.21957/MLK72GJ183. URL <https://www.ecmwf.int/node/19843>. Publisher: ECMWF.
- Christian M. Grams, Remo Beerli, Stefan Pfenninger, Iain Staffell, and Heini Wernli. Balancing Europe's wind-power output through spatial deployment informed by weather regimes. *Nature Climate Change*, 7(8):557–562, August 2017. ISSN 1758-6798. doi: 10.1038/nclimate3338. URL <https://www.nature.com/articles/nclimate3338>. Publisher: Nature Publishing Group.
- Richard J. Hall and Edward Hanna. North Atlantic circulation indices: links with summer and winter UK temperature and precipitation and implications for seasonal forecasting. *International Journal of Climatology*, 38(S1):e660–e677, 2018. ISSN 1097-0088. doi: 10.1002/joc.5398. URL <https://onlinelibrary.wiley.com/doi/abs/10.1002/joc.5398>. _eprint: <https://onlinelibrary.wiley.com/doi/pdf/10.1002/joc.5398>.
- Richard J. Hall, Hua-Liang Wei, and Edward Hanna. Complex systems modelling for statistical forecasting of winter North Atlantic atmospheric variability: A new approach to North Atlantic seasonal forecasting. *Quarterly Journal of the Royal Meteorological Society*, 145(723):2568–2585, 2019. ISSN 1477-870X. doi: 10.1002/qj.3579. URL <https://onlinelibrary.wiley.com/doi/abs/10.1002/qj.3579>. _eprint: <https://onlinelibrary.wiley.com/doi/pdf/10.1002/qj.3579>.
- A. Hannachi, I. T. Jolliffe, and D. B. Stephenson. Empirical orthogonal functions and related techniques in atmospheric science: A review. *International Journal of Climatology*, 27(9):1119–1152, 2007. ISSN 1097-0088. doi: 10.1002/joc.1499. URL <https://onlinelibrary.wiley.com/doi/abs/10.1002/joc.1499>. _eprint: <https://onlinelibrary.wiley.com/doi/pdf/10.1002/joc.1499>.
- Abdel. Hannachi, David M. Straus, Christian L. E. Franzke, Susanna Corti, and Tim Woollings. Low-frequency nonlinearity and regime behavior in the Northern Hemisphere extratropical atmosphere. *Reviews of Geophysics*, 55(1):199–234, 2017. ISSN 1944-9208. doi: 10.1002/2015RG000509. URL <https://onlinelibrary.wiley.com/doi/abs/10.1002/2015RG000509>. _eprint: <https://onlinelibrary.wiley.com/doi/pdf/10.1002/2015RG000509>.
- H. Hersbach, E. Comyn-Platt, B. Bell, P. Berrisford, G. Biavati, A. Horányi, J. Muñoz Sabater, J. Nicolas, C. Peubey, R. Radu, I. Rozum, D. Schepers, A. Simmons, C. Soci, D. Dee, J.-N. Thépaut, C. Cagnazo, and M. Cucchi. Era5 post-processed daily-statistics on pressure levels from 1940 to present, 2023. Accessed on 23rd January 2025.
- H. Hersbach, B. Bell, P. Berrisford, G. Biavati, A. Horányi, J. Muñoz Sabater, J. Nicolas, C. Peubey, R. Radu, I. Rozum, D. Schepers, A. Simmons, C. Soci, D. Dee, and J.-N. Thépaut. Copernicus climate change service, climate data store, (2024): Era5 post-processed daily-statistics on

- pressure levels from 1940 to present, 2024a. Accessed on 23rd January 2025.
- H. Hersbach, B. Bell, P. Berrisford, G. Biavati, A. Horányi, J. Muñoz Sabater, J. Nicolas, C. Peubey, R. Radu, I. Rozum, D. Schepers, A. Simmons, C. Soci, D. Dee, and J-N. Thépaut. Copernicus climate change service, climate data store, (2024): Era5 post-processed daily-statistics on single levels from 1940 to present, 2024b. Accessed on 23rd January 2025.
- Hans Hersbach. Decomposition of the continuous ranked probability score for ensemble prediction systems. *Weather and Forecasting*, 15(5):559 – 570, 2000. doi: 10.1175/1520-0434(2000)015<0559:DOTCRP>2.0.CO;2. URL https://journals.ametsoc.org/view/journals/wefo/15/5/1520-0434_2000_015_0559_dotcrp_2_0_co_2.xml.
- Hans Hersbach, Bill Bell, Paul Berrisford, Shoji Hirahara, András Horányi, Joaquín Muñoz-Sabater, Julien Nicolas, Carole Peubey, Raluca Radu, Dinand Schepers, Adrian Simmons, Cornel Soci, Saleh Abdalla, Xavier Abellan, Gianpaolo Balsamo, Peter Bechtold, Gionata Biavati, Jean Bidlot, Massimo Bonavita, Giovanna De Chiara, Per Dahlgren, Dick Dee, Michail Diamantakis, Rossana Dragani, Johannes Flemming, Richard Forbes, Manuel Fuentes, Alan Geer, Leo Haimberger, Sean Healy, Robin J. Hogan, Elias Hölm, Marta Janisková, Sarah Keeley, Patrick Laloyaux, Philippe Lopez, Cristina Lupu, Gabor Radnoti, Patricia de Rosnay, Iryna Rozum, Freja Vamborg, Sebastien Vilaume, and Jean-Noël Thépaut. The era5 global reanalysis. *Quarterly Journal of the Royal Meteorological Society*, 146(730):1999–2049, 2020. doi: <https://doi.org/10.1002/qj.3803>. URL <https://rmets.onlinelibrary.wiley.com/doi/abs/10.1002/qj.3803>.
- Assaf Hochman, Gabriele Messori, Julian F. Quinting, Joaquim G. Pinto, and Christian M. Grams. Do Atlantic-European Weather Regimes Physically Exist? *Geophysical Research Letters*, 48(20):e2021GL095574, 2021. ISSN 1944-8007. doi: 10.1029/2021GL095574. URL <https://onlinelibrary.wiley.com/doi/abs/10.1029/2021GL095574>. eprint: <https://onlinelibrary.wiley.com/doi/pdf/10.1029/2021GL095574>.
- James W. Hurrell, Yochanan Kushnir, Geir Ottersen, and Martin Visbeck. An Overview of the North Atlantic Oscillation. In *The North Atlantic Oscillation: Climatic Significance and Environmental Impact*, pages 1–35. American Geophysical Union (AGU), 2003. ISBN 978-1-118-66903-7. doi: 10.1029/134GM01. URL <https://onlinelibrary.wiley.com/doi/abs/10.1029/134GM01>. eprint: <https://onlinelibrary.wiley.com/doi/pdf/10.1029/134GM01>.
- Stephanie J. Johnson, Timothy N. Stockdale, Laura Ferranti, Magdalena A. Balmaseda, Franco Molteni, Linus Magnusson, Steffen Tietsche, Damien Decremer, Antje Weisheimer, Gianpaolo Balsamo, Sarah P. E. Keeley, Kristian Mogensen, Hao Zuo, and Beatriz M. Monge-Sanz. SEAS5: the new ECMWF seasonal forecast system. *Geoscientific Model Development*, 12(3):1087–1117, March 2019. ISSN 1991-959X. doi: 10.5194/gmd-12-1087-2019. URL <https://gmd.copernicus.org/articles/12/1087/2019/>. Publisher: Copernicus GmbH.
- Diederik P. Kingma and Jimmy Ba. Adam: A method for stochastic optimization, 2017. URL <https://arxiv.org/abs/1412.6980>.
- Randal D. Koster, Max J. Suarez, and Mark Heiser. Variance and predictability of precipitation at seasonal-to-interannual timescales. *Journal of Hydrometeorology*, 1(1):26 – 46, 2000. doi: 10.1175/1525-7541(2000)001<0026:VAPOPA>2.0.CO;2. URL https://journals.ametsoc.org/view/journals/hydr/1/1/1525-7541_2000_001_0026_vapopa_2_0_co_2.xml.
- Folmer Krikken, Gertie Geertsema, Kristian Nielsen, and Alberto Troccoli. The added value of statistical seasonal forecasts. *Climate*, 12(6), 2024. ISSN 2225-1154. doi: 10.3390/cli12060083. URL <https://www.mdpi.com/2225-1154/12/6/83>.
- Simon H. Lee, Michael K. Tippett, and Lorenzo M. Polvani. A new year-round weather regime classification for north america. *Journal of Climate*, 36(20):7091 – 7108, 2023. doi: 10.1175/JCLI-D-23-0214.1. URL <https://journals.ametsoc.org/view/journals/clim/36/20/JCLI-D-23-0214.1.xml>.
- Edward N. Lorenz. Deterministic Nonperiodic Flow. *Journal of Atmospheric Sciences*, March 1963. ISSN 1520-0469. URL https://journals.ametsoc.org/view/journals/atsc/20/2/1520-0469_1963_020_0130_dnf_2_0_co_2.xml. Section: Journal of the Atmospheric Sciences.
- Erica Madonna, David S. Battisti, Camille Li, and Rachel H. White. Reconstructing winter climate anomalies in the Euro-Atlantic sector using circulation patterns. *Weather and Climate Dynamics*, 2(3):777–794, August 2021. doi: 10.5194/wcd-2-777-2021. URL <https://wcd.copernicus.org/articles/2/777/2021/>. Publisher: Copernicus GmbH.
- Nikolaos Mastrantonas, Pedro Herrera-Lormendez, Linus Magnusson, Florian Pappenberger, and Jörg Matschullat. Extreme precipitation events in the Mediterranean: Spatiotemporal characteristics and connection to large-scale atmospheric flow patterns. *International Journal of*

- Climatology*, 41(4):2710–2728, 2021. ISSN 1097-0088. doi: 10.1002/joc.6985. URL <https://onlinelibrary.wiley.com/doi/abs/10.1002/joc.6985>. _eprint: <https://onlinelibrary.wiley.com/doi/pdf/10.1002/joc.6985>.
- Clio Michel and Gwendal Rivière. The Link between Rossby Wave Breakings and Weather Regime Transitions. *J. Atmos. Sci.*, August 2011. doi: 10.1175/2011JAS3635.1. URL <https://journals.ametsoc.org/view/journals/atasc/68/8/2011jas3635.1.xml>. Section: Journal of the Atmospheric Sciences.
- Paul-Antoine Michelangeli, Robert Vautard, and Bernard Legras. Weather regimes: Recurrence and quasi stationarity. *Journal of Atmospheric Sciences*, 52(8):1237 – 1256, 1995. doi: 10.1175/1520-0469(1995)052<1237:WRRFAQS>2.0.CO;2. URL https://journals.ametsoc.org/view/journals/atasc/52/8/1520-0469_1995_052_1237_wrraqs_2_0_co_2.xml.
- Niti Mishra, Chloé Prodhomme, and Virginie Guemas. Multi-model skill assessment of seasonal temperature and precipitation forecasts over Europe. *Climate Dynamics*, 52(7):4207–4225, April 2019. ISSN 1432-0894. doi: 10.1007/s00382-018-4404-z. URL <https://doi.org/10.1007/s00382-018-4404-z>.
- Dmitry Mukhin, Abdel Hannachi, Tobias Braun, and Norbert Marwan. Revealing recurrent regimes of mid-latitude atmospheric variability using novel machine learning method, January 2024a. URL <http://arxiv.org/abs/2401.10073>. arXiv:2401.10073.
- Dmitry Mukhin, Roman Samoilov, and Abdel Hannachi. Metastability, atmospheric midlatitude circulation regimes and large-scale teleconnection: a data-driven approach, December 2024b. URL <http://arxiv.org/abs/2412.06933>. arXiv:2412.06933 [physics].
- Andreas Holm Nielsen, Alexandros Iosifidis, and Henrik Karstoft. Forecasting large-scale circulation regimes using deformable convolutional neural networks and global spatiotemporal climate data. *Scientific Reports*, 12(1):8395, May 2022. ISSN 2045-2322. doi: 10.1038/s41598-022-12167-8. URL <https://www.nature.com/articles/s41598-022-12167-8>. Publisher: Nature Publishing Group.
- Geert De Paepe and Lesley De Cruz. Diresa, a distance-preserving nonlinear dimension reduction technique based on regularized autoencoders, 2025. URL <https://arxiv.org/abs/2404.18314>.
- T. N. Palmer, A. Alessandri, U. Andersen, P. Cantelaube, M. Davey, P. Décluse, M. Déqué, E. Díez, F. J. Doblas-Reyes, H. Feddersen, R. Graham, S. Gualdi, J.-F. Guérémy, R. Hagedorn, M. Hoshen, N. Keenlyside, M. Latif, A. Lazar, E. Maisonnavé, V. Marletto, A. P. Morse, B. Orfila, P. Rogel, J.-M. Terres, and M. C. Thomson. DEVELOPMENT OF A EUROPEAN MULTIMODEL ENSEMBLE SYSTEM FOR SEASONAL-TO-INTERANNUAL PREDICTION (DEMETER). *Bulletin of the American Meteorological Society*, 85(6):853–872, June 2004. ISSN 0003-0007, 1520-0477. doi: 10.1175/BAMS-85-6-853. URL <https://journals.ametsoc.org/view/journals/bams/85/6/bams-85-6-853.xml>. Publisher: American Meteorological Society Section: Bulletin of the American Meteorological Society.
- Guy Plaut and Eric Simonnet. Large-scale circulation classification, weather regimes, and local climate over France, the Alps and Western Europe. *Climate Research*, 17(3): 303–324, August 2001. ISSN 0936-577X, 1616-1572. doi: 10.3354/cr017303. URL <https://www.int-res.com/abstracts/cr/v17/n3/p303-324/>.
- Dian Nur Ratri, Kirien Whan, and Maurice Schmeits. Calibration of ECMWF Seasonal Ensemble Precipitation Forecasts in Java (Indonesia) Using Bias-Corrected Precipitation and Climate Indices. *Weather and Forecasting*, August 2021. doi: 10.1175/WAF-D-20-0124.1. URL <https://journals.ametsoc.org/view/journals/wefo/36/4/waf-d-20-0124.1.xml>. Section: Weather and Forecasting.
- Kevin J. Rennert and John M. Wallace. Cross-Frequency Coupling, Skewness, and Blocking in the Northern Hemisphere Winter Circulation. *Journal of Climate*, November 2009. doi: 10.1175/2009JCLI2669.1. URL <https://journals.ametsoc.org/view/journals/clim/22/21/2009jcli2669.1.xml>. Section: Journal of Climate.
- Daniel F. Rex. The Effect of Atlantic Blocking Action upon European Climate. *Tellus*, 3(2):100–112, 1951. ISSN 2153-3490. doi: 10.1111/j.2153-3490.1951.tb00784.x. URL <https://onlinelibrary.wiley.com/doi/abs/10.1111/j.2153-3490.1951.tb00784.x>. _eprint: <https://onlinelibrary.wiley.com/doi/pdf/10.1111/j.2153-3490.1951.tb00784.x>.
- N. Rieger and S. J. Levang. xeofs: Comprehensive eof analysis in python with xarray. *Journal of Open Source Software*, 9(93), 2024. doi: 10.21105/joss.06060. URL <https://doi.org/10.21105/joss.06060>.
- Christopher D. Roberts, Magdalena A. Balmaseda, Laura Ferranti, and Frederic Vitart. Euro-Atlantic Weather

- Regimes and Their Modulation by Tropospheric and Stratospheric Teleconnection Pathways in ECMWF Reforecasts. *Monthly Weather Review*, 151, October 2023. doi: 10.1175/MWR-D-22-0346.1. URL <https://journals.ametsoc.org/view/journals/mwre/151/10/MWR-D-22-0346.1.xml>. Section: Monthly Weather Review.
- Andrew W. Robertson, Nicolas Vigaud, Jing Yuan, and Michael K. Tippett. Toward identifying subseasonal forecasts of opportunity using north american weather regimes. *Monthly Weather Review*, 148(5):1861 – 1875, 2020. doi: 10.1175/MWR-D-19-0285.1. URL <https://journals.ametsoc.org/view/journals/mwre/148/5/mwr-d-19-0285.1.xml>.
- C.-G. Rossby. Planetary flow patterns in the atmosphere. *Quarterly Journal of the Royal Meteorological Society*, 66(51):68–87, 1940. doi: <https://doi.org/10.1002/j.1477-870X.1940.tb00130.x>. URL <https://rmets.onlinelibrary.wiley.com/doi/abs/10.1002/j.1477-870X.1940.tb00130.x>.
- Luis Samaniego, Stephan Thober, Niko Wanders, Ming Pan, Oldrich Rakovec, Justin Sheffield, Eric F. Wood, Christel Prudhomme, Gwyn Rees, Helen Houghton-Carr, Matthew Fry, Katie Smith, Glenn Watts, Hege Hisdal, Teodoro Estrela, Carlo Buontempo, Andreas Marx, and Rohini Kumar. Hydrological forecasts and projections for improved decision-making in the water sector in europe. *Bulletin of the American Meteorological Society*, 100(12): 2451 – 2472, 2019. doi: 10.1175/BAMS-D-17-0274.1. URL <https://journals.ametsoc.org/view/journals/bams/100/12/bams-d-17-0274.1.xml>.
- Katherine E. Schlef, Hamid Moradkhani, and Upmanu Lall. Atmospheric Circulation Patterns Associated with Extreme United States Floods Identified via Machine Learning. *Scientific Reports*, 9(1):7171, May 2019. ISSN 2045-2322. doi: 10.1038/s41598-019-43496-w. URL <https://www.nature.com/articles/s41598-019-43496-w>. Publisher: Nature Publishing Group.
- Siegfried Schubert, Hailan Wang, and Max Suarez. Warm season subseasonal variability and climate extremes in the northern hemisphere: The role of stationary rossby waves. *Journal of Climate*, 24(18):4773 – 4792, 2011. doi: 10.1175/JCLI-D-10-05035.1. URL <https://journals.ametsoc.org/view/journals/clim/24/18/jcli-d-10-05035.1.xml>.
- Ian Simpson, Edward Hanna, Laura Baker, Yiming Sun, and Hua-Liang Wei. North Atlantic atmospheric circulation indices: Links with summer and winter temperature and precipitation in north-west Europe, including persistence and variability. *International Journal of Climatology*, 44(3):902–922, 2024. ISSN 1097-0088. doi: 10.1002/joc.8364. URL <https://onlinelibrary.wiley.com/doi/abs/10.1002/joc.8364>. _eprint: <https://onlinelibrary.wiley.com/doi/pdf/10.1002/joc.8364>.
- Sebastian Springer, Alessandro Laio, Vera Melinda Galfi, and Valerio Lucarini. Unsupervised detection of large-scale weather patterns in the northern hemisphere via Markov State Modelling: from blockings to teleconnections. *npj Climate and Atmospheric Science*, 7(1):1–13, May 2024. ISSN 2397-3722. doi: 10.1038/s41612-024-00659-5. URL <https://www.nature.com/articles/s41612-024-00659-5>. Publisher: Nature Publishing Group.
- Fiona R. Spuler, Marlene Kretschmer, Yevgeniya Kovalchuk, Magdalena Alonso Balmaseda, and Theodore G. Shepherd. Identifying probabilistic weather regimes targeted to a local-scale impact variable. *Environmental Data Science*, 3:e25, January 2024. ISSN 2634-4602. doi: 10.1017/eds.2024.29. URL <https://www.cambridge.org/core/journals/environmental-data-science/article/identifying-probabilistic-weather-regimes-targeted-to-a-localscale-impact-variable/DOF1F80FE4ACD2B85F4651FF69F1ED0B>.
- Kristian Strommen, Matthew Chantry, Joshua Dorrington, and Nina Otter. A topological perspective on weather regimes. *Climate Dynamics*, 60(5):1415–1445, March 2023. ISSN 1432-0894. doi: 10.1007/s00382-022-06395-x. URL <https://doi.org/10.1007/s00382-022-06395-x>.
- Ricardo M. Trigo and Carlos C. DaCamara. Circulation weather types and their influence on the precipitation regime in Portugal. *International Journal of Climatology*, 20(13):1559–1581, 2000. ISSN 1097-0088. doi: 10.1002/1097-0088(20001115)20:13<1559::AID-JOC555>3.0.CO;2-5. URL <https://onlinelibrary.wiley.com/doi/abs/10.1002/1097-0088%2820001115%2920%3A13%3C1559%3A%3AAID-JOC555%3E3.0.CO%3B2-5>. _eprint: <https://onlinelibrary.wiley.com/doi/pdf/10.1002/1097-0088%2820001115%2920%3A13%3C1559%3A%3AAID-JOC555%3E3.0.CO%3B2-5>.
- Ricardo M. Trigo, Timothy J. Osborn, and João M. Corte-Real. The north atlantic oscillation influence on europe: climate impacts and associated physical mechanisms. *Climate Research*, 20(1):9–17, 2002. ISSN 0936577X, 16161572. URL <http://www.jstor.org/stable/24866789>.
- Karin van der Wiel, Hannah C Bloomfield, Robert W Lee, Laurens P Stoop, Russell Blackport, James A Screen,

and Frank M Selten. The influence of weather regimes on European renewable energy production and demand. *Environmental Research Letters*, 14(9):094010, September 2019. ISSN 1748-9326. doi: 10.1088/1748-9326/ab38d3. URL <https://dx.doi.org/10.1088/1748-9326/ab38d3>. Publisher: IOP Publishing.

R. Vautard, P. Yiou, F. D'Andrea, N. de Noblet, N. Viovy, C. Cassou, J. Polcher, P. Ciais, M. Kageyama, and Y. Fan. Summertime European heat and drought waves induced by wintertime Mediterranean rainfall deficit. *Geophysical Research Letters*, 34(7), 2007. ISSN 1944-8007. doi: 10.1029/2006GL028001. URL <https://onlinelibrary.wiley.com/doi/abs/10.1029/2006GL028001>. eprint: <https://onlinelibrary.wiley.com/doi/pdf/10.1029/2006GL028001>

John M. Wallace and David S. Gutzler. Teleconnections in the Geopotential Height Field during the Northern Hemisphere Winter. *American Meteorological Society, Monthly Weather Review*(109):784 - 812, April 1981. ISSN 1520-0493. doi: 10.1175/1520-0493(1981)109<0784:TITGHF>2.0.CO;2. URL https://journals.ametsoc.org/view/journals/mwre/109/4/1520-0493_1981_109_0784_titghf_2_0_co_2.xml. Section: Monthly Weather Review.

Omry Yadan. Hydra - a framework for elegantly configuring complex applications. Github, 2019. URL <https://github.com/facebookresearch/hydra>.

Appendix

A | FOUR WINTER AND SUMMER WR

We compute the four WR for winter and summer using the same methodology described in Sec. 3.1, with the only change being the number of centroids used to cluster the data. The mean Z500 field (black isocontours) and the corresponding average Z500 anomalies during winter (December, January, February) and summer (June, July, August), associated with the four Euro-Atlantic WR, are presented in Fig. A.1 and Fig. A.2, respectively. The four WR are the ZO, ScBL, AT and GL.

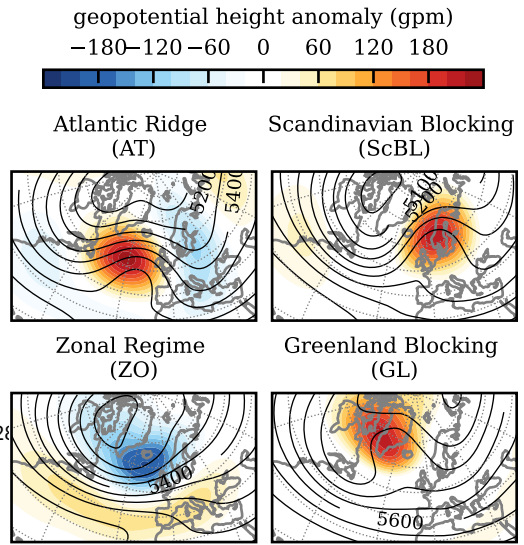


FIGURE A.1 Cluster mean of the Z500 field (black isocontours) and corresponding average Z500 anomalies in winter (December, January, February), associated with the four Euro-Atlantic WR. The average is performed in the 1981-2010 climatology.

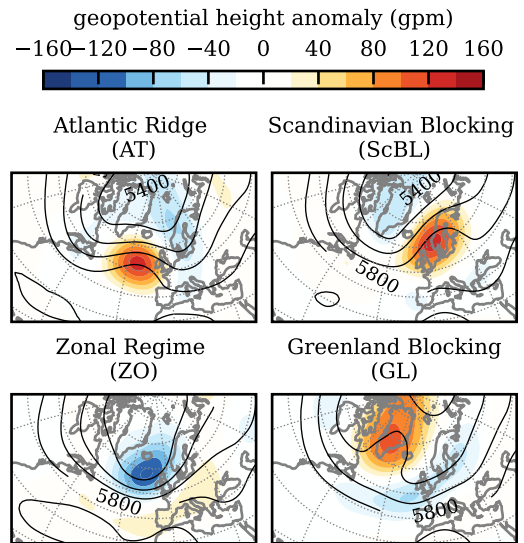


FIGURE A.2 Cluster mean of the Z500 field (black isocontours) and corresponding average Z500 anomalies in summer (June, July, August), associated with the four Euro-Atlantic WR. The average is performed in the 1981-2010 climatology.

B | DIFFERENCES IN THE WR COMPUTATIONS RELATIVE TO GRAMS ET AL. (2017)

We now highlight the major differences to the procedure described in Grams et al. (2017) and in Büeler et al. (2021). The authors of the mentioned work used the ERA-Interim reanalysis (Dee et al., 2011) six-hourly 500 hPa GPH from 11 January 1971 to 31 December 2015; we instead use ERA5 daily 500 hPa GPH from 1st of January 1940 to 31 December 2024. Moreover, the anomalies computation, the EOF analysis, the K-means clustering, and the definition of the cluster's mean field are performed only in the climatology period. (Grams et al., 2017) applied 90- and 30-day moving window averages to smooth the calendar day mean and standard deviation. In contrast, we use a 15-day centered moving average for each calendar day. We observed that using window sizes larger than approximately 30 days tends to preserve seasonal trends in the resulting anomalies. This explains the minor difference that can be found when comparing Fig. 1 with the corresponding Supplementary Figure 1 in Grams et al. (2017) and Figure 1 in Büeler et al. (2021).

C | TRAINING SETUP AND HYPERPARAMETERS

The models are trained using mean squared error (MSE) as the loss function (see Sec. 4.2). Training is performed using the Adam optimizer (Kingma and Ba, 2017) with minibatches and early stopping based on the minimum validation loss, so the total number of epochs varies between runs and is not fixed *a priori*. We employ a learning-rate plateau scheduler: whenever the validation loss does not improve for 10 consecutive epochs, the learning rate is reduced by a factor of 0.5. The network includes dropout with a dropout rate of 0.2 to mitigate overfitting. Other training hyperparameters are reported in Tab. C.0. Within reasonable ranges, hyperparameters such as batch size, initial learning rate, patience, and dropout rate have a limited impact on the final performance of the models. In our experiments, variations in these quantities result in

TABLE C.0 Summary of training hyperparameters used in this work.

Hyperparameter	Value
Loss function	MSE
Optimizer	Adam
Initial learning rate	10^{-3}
LR reduction factor	0.5
LR plateau patience	10 epochs
Batch size	8
Dropout rate	0.2

changes comparable to the run-to-run variability due to randomness (see Tables 1 and 2).

D | ANOMALY RECONSTRUCTION WITHOUT INDICES

As a baseline for evaluating the added value of the WR indices, we trained the same AI model described in Sec. 4 to reconstruct monthly mean two-meter temperature and total precipitation anomalies without including the WR indices as input. The obtained spatial ACC and CE for the winter mean two-meter temperature and total precipitation anomalies are shown in Fig. D.1. Despite the absence of synoptic-scale information, the model exhibits low but positive ACC in certain European regions, likely due to its ability to learn and exploit the underlying climate trend present in the training data. Nevertheless, the CE value is close to zero or negative, indicating that the model is unable to replicate the amplitude of the fluctuations in the test dataset.

E | EVALUATION OF THE SEAS5 WR FORECAST

As noted in Sec. 5.5, the low skills of the AI model driven by the SEAS5 forecasted WR indices, I_{WR}^{SEAS5} , suggest that the SEAS5 forecast of the WR indices is not very skillful. Fig. E.1 show the CRPS (lower is better) and the

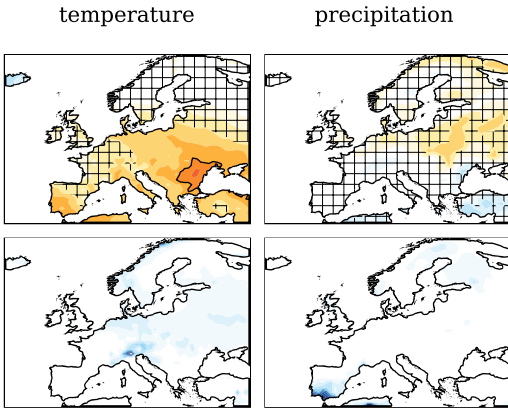


FIGURE D.1 Spatial ACC (top) and CE (bottom) of the AI model reconstruction of the winter mean two-meter temperature and total precipitation anomalies without using the information encoded in the WR indices. The skills are computed in the test years (from January 2011 to 2024. Hatched areas mark regions with correlations that are not significant at $p > 0.05$. Black contours indicate regions with ACC higher than 0.5.

ensemble mean correlation (higher is better) between I_{wr}^{SEAS5} and I_{wr} , i.e. between the monthly indices forecasted by the bias corrected SEAS5 and the indices computed from ERA5 Z500 (see Sec. 3.1 and Sec. 3.4). Both the CRPS and the ensemble mean correlation are good in the initialization month, but the skill degrades abruptly from the second forecasted month. As usually done in the literature, we initialize SEAS5 in November for winter forecasts (DJF), and in May for summer forecasts (JJA). The considered forecast is relative to the second, third, and fourth forecasted months, which, in general, has poor skills.

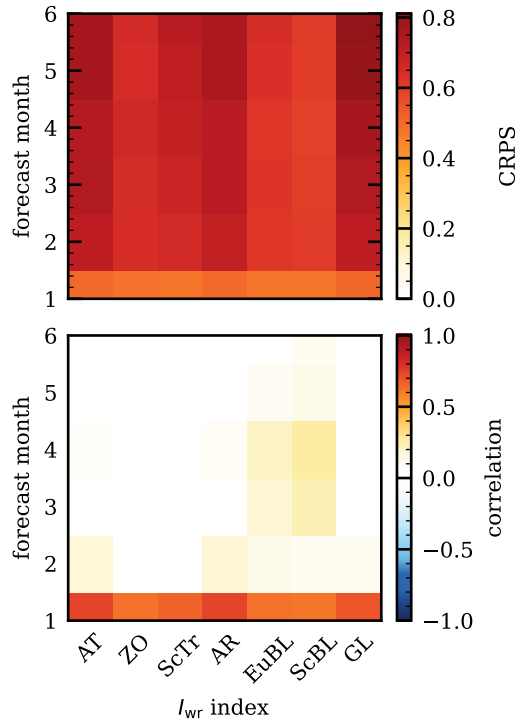


FIGURE E.1 CRPS (lower is better) and ensemble mean correlation (higher is better) of SEAS5 WR indices forecast, I_{wr}^{SEAS5} , with respect to ERA5 WR indices, I_{wr} . The labels refer to the WR names: AT, ZO, ST, AR, EuBL, ScBL, GL.